AD-A170 299 STABLE CRACK GROWTH IN ALUMINUM TENSILE SPECIMENS(U) 1/1
WASHINGTON UNIV SEATTLE DEPT OF MECHANICAL ENGINEERING
B S KANG ET AL. JUL 86 UWA/DME/TR-86/54
UNCLASSIFIED N00014-85-K-0187 F/G 11/6 NL

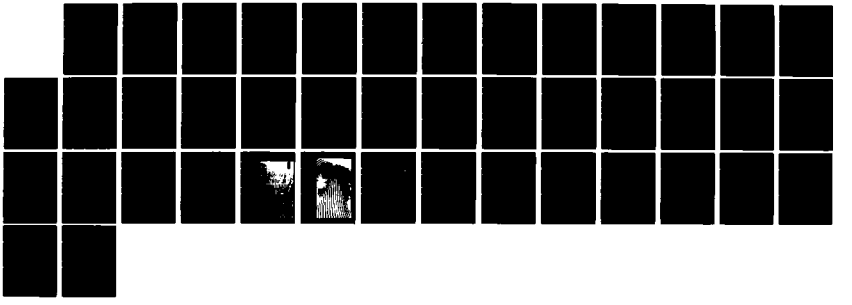

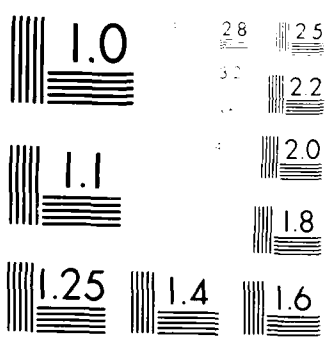
1.0
2.8
2.5
2.2
1.1
2.0
1.8
1.25
1.4
1.6

(4)

Office of Naval Research

Contract N00014-85-K-0187

Technical Report No. UWA/DME/TR-86/54

STABLE CRACK GROWTH IN ALUMINUM TENSILE SPECIMENS

by

B.S.-J. Kang, A.S. Kobayashi and D. Post

July 1986

The research reported in this technical report was made possible through support extended to the Department of Mechanical Engineering, University of Washington, by the Office of Naval Research under Contract N00014-85-K-0187. Reproduction in whole or in part is permitted for any purpose of the United States Government.

STABLE CRACK GROWTH IN ALUMINUM TENSILE SPECIMENS

B.S.-J. Kang*, A.S. Kobayashi* and D. Post**

ABSTRACT

Post's white light moire interferometry was used to obtain sequential records of the transient u_y-displacement fields associated with stable crack growth in 7075-T6 and 2024-0, single edge notched (SEN) specimens with fatigued cracks. The u_y-displacement fields were used to evaluate the crack tip opening displacement (CTOD), far and near-field J-integral values, Dugdale strip yield model, William's polynomial function and the HRR fields.

INTRODUCTION

Crack growth in ductile material can be divided into three stages, namely, 1) plastic yielding and the onset of stable crack growth, 2) stable crack growth and 3) rapid tearing. Since the measured crack velocity during rapid tearing is less than 5 percent of the dilatational wave velocity [1,2,3], rapid tearing and stable crack growth can be considered as quasi-static deformation processes. The crack-tip state for rapidly tearing and stably growing cracks, however, are different from that of a stationary crack. Asymptotic analyses of a stationary crack in an elastic, perfectly plastic solid under infinitesimal deformation show that the strains vary as $1/r$ but for a growing crack the strains vary as $\ln(1/r)$ [4-8]. On the other hand, numerical studies [9-13] on stable crack growth do not address the crack tip singularity problem but discuss the somewhat near stress field surrounding the crack tip.

Numerous fracture parameters which characterize stable crack growth under small-scale yielding condition, such as average crack opening angle (COA) [14],

* University of Washington, Department of Mechanical Engineering, Seattle, WA 98195.
** Virginia Polytechnic Institute and State University, Department of Engineering Science and Mechanics, Blacksburg, VA 24061.

crack tip opening angle (CTOA) [15], crack tip opening displacement (CTOD) [16], critical strain [17,18], energy release rate [19], crack tip force [20], J-resistance curve [21] and tearing modulus (T) [22], have been proposed. Of these, the crack tip opening angle (CTOA) or displacement (CTOD) was shown to be suited for modeling stable crack growth and instability during the fracture process [15,20,21].

Under large-scale yielding condition, however, there is no analytical solution available for stable crack growth. Attempts have been made to extend the ductile fracture criteria for small-scale yielding and stable crack growth to large-scale yielding. The few results published to date [1,2,15,20] indicate that under limited conditions, the CTOA or CTOD, are plausible ductile fracture criteria. The purpose of this paper is to present preliminary experimental findings on the crack tip parameters which control the initiation and propagation of stable crack growth. An approximate J-integral evaluation procedure based on u_y-displacement field is also presented.

ANALYTICAL BACKGROUND

(1) J-integral

For two-dimensional problems of materials governed by nonlinear elasticity and deformation plasticity theory subjected to monotonically loading condition, the J-integral is defined as [23]

$$J = \int_\Gamma W\, dy - \vec{T} \cdot \frac{\partial \vec{u}}{\partial x}\, ds \qquad (1)$$

where

Γ : contour surrounding the crack tip
$\vec{T}$: traction vector along the contour
$\vec{u}$: displacement vector on the contour
W : strain energy density on the contour

In the following, an experimental procedure for direct far-field and approximate near-field J-integral measurement is introduced. The underlining methodology is to compute the J value with only the u_y-displacement field which is obtained from a single moire interferometry recording.

Far-field J-integral Measurement

Consider a line-integration contour in a single edge notched (SEN) specimen subjected to Mode I loading condition as shown in Figure 1. Due to symmetry, only half of the contour is needed for J calculation.

Along the vertical segment 12, 34, which are free surfaces, the second term of the integrand as well as all stress components except σ_{yy}, which is subject to unaxial tension, in W vanish. Thus, the strain energy density, W, along 12, 34 is

$$W = \int \sigma_{yy} \, d\varepsilon_{yy}$$

For an elastic field, $\sigma_{yy} = \varepsilon_{yy} * E$ and $W = \frac{1}{2} E \varepsilon_{yy}^2$, where E is the modulus of of elasticity. Under plastic yielding, e.g., $\varepsilon_{yy} > \frac{\sigma_o}{E}$, the following two cases are considered. For an elastic, perfectly plastic material,

$$\sigma_{yy} = \sigma_o \tag{2a}$$

and

$$W = \frac{1}{2} \frac{\sigma_o^2}{E} + \sigma_o(\varepsilon_{yy} - \frac{\sigma_o}{E}) \tag{2b}$$

For a power hardening material,

$$\varepsilon_{yy} = \frac{\sigma_{yy}}{E} + \alpha \frac{\sigma_{yy}}{E} \left(\frac{\sigma_{yy}}{\sigma_o} \right)^{N-1} \tag{2c}$$

and

$$W = \frac{1}{2}\frac{\sigma_{yy}^2}{E} + \frac{N}{N+1}\frac{\alpha}{E}\sigma_{yy}^2\left(\frac{\sigma_{yy}}{\sigma_o}\right)^{N-1} \tag{2d}$$

where σ_o is the yield stress, N is the strain hardening constant and α is a dimensionless material constant, σ_{yy} is calculated from Equation (2c) for a given ε_{yy} which can be determined experimentally from the moire data.

Thus the integral value of Equation (1) along the vertical edges of segments $\underline{12}$ and $\underline{34}$, is

$$J_v = \int_{\underline{12}+\underline{34}} W\, dy$$

$$= (\Sigma W_i\, \Delta y_i)_{\underline{12}} + (\Sigma W_i\, \Delta y_i)_{\underline{34}} \tag{3}$$

where i is the ith segment of the contour.

Along the horizontal segment $\underline{23}$, dy is zero and the first term of the integrand in Equation (1) vanishes. The traction, $\vec{T}$, along this segment are $T_y = \sigma_{yy}$ and $T_x = \tau_{xy}$. At this point we assume that the shear stress, τ_{xy}, and the displacement, u_x, are negligible along segment $\underline{23}$. This assumption is justified if segment $\underline{23}$ is sufficiently far away from the crack. The integral value of Equation (1) along segment $\underline{23}$ thus becomes

$$J_h = \int_{\underline{23}} T_y \cdot \frac{\partial u_y}{\partial x}\, dx$$

$$= \Sigma\left[\left(\sigma_{yy} \cdot \frac{\Delta u_y}{\Delta x}\right)_i \Delta x_i\right]_{\underline{23}} \tag{4}$$

Again, for the σ_{yy} term, the same stress-strain relation, e.g., Equations (2) is used. Finally, the J-integral value is given by

$$J = 2(J_v + J_h) \tag{5}$$

The above experimental procedure for determining J-integral value was carried out using strain gages and linear variable displacement transducers at discrete points along the specimen boundary [24-26]. Since the test data in these references were obtained from few locations, Equation (5) could only be evaluated at a few discrete locations. Moire interferometry, on the other hand, provides an easy alternative for implementing this method with better accuracy. Since it yields highly sensitive displacement field, the approximate analysis proposed above requires only a single u_y-displacement moire field for calculating the J-integral.

Near-field J-integral Measurement

While the above procedure is valid for far-field J-integral evaluation, its validity for the near field integration contour, such as the inside rectangular contour shown in Figure 1, must be justified. First, we will show that the above far field J-integral measurement procedure is a reasonable approximation for the near-field J value in a linear elastic field.

Consider a rectangular contour around the crack tip as shown in the legend of Figure 2. For a linearly elastic material, the J integral along the horizontal segment 13 can be expressed in terms of displacements u_x and u_y as

$$J_h = \int_h \left\{ -2G M_1 \frac{\partial u_y}{\partial y} \frac{\partial u_y}{\partial x} - G \frac{\partial u_x}{\partial x} \left(\frac{\partial u_x}{\partial y} + M_2 \frac{\partial u_y}{\partial x} \right) \right\} dx \qquad (6a)$$

Along the two vertical segments, 01 and 34,

$$J_v = \int_v \left\{ G M_1 \left(\frac{\partial u_y}{\partial y} \right)^2 + G \left[\frac{1}{2} \left(\frac{\partial u_x}{\partial y} + \frac{\partial u_y}{\partial x} \right) \left(\frac{\partial u_x}{\partial y} - \frac{\partial u_y}{\partial x} \right) - M_1 \left(\frac{\partial u_x}{\partial x} \right)^2 \right] \right\} dy \qquad (6b)$$

where G is the shear modulus, ν is the Poisson's ratio and

$$M_1 = \begin{cases} \dfrac{1}{1-\nu} & \text{(plane stress)} \\ \dfrac{1-\nu}{1-2\nu} & \text{(plane strain)} \end{cases} \tag{6c}$$

$$M_2 = (2M_1 - 1) \tag{6d}$$

The second term of the integrand in Equations (6a) and (6b) were neglected in evaluating the far-field J-integral. For the near-field J-integral evaluation, we will also assume that the contour integrals, as represented by Equation (3) and (4), can be used. The error due to such assumption is evaluated in the following.

Consider a crack in a two dimensional linear elastic material. The mode I crack -tip displacements are

$$u_x = \frac{K_I}{G}\frac{\sqrt{r}}{\sqrt{2\pi}} \cos\frac{\theta}{2}\left[M_3 + \sin^2\frac{\theta}{2}\right] \tag{7a}$$

$$u_y = \frac{K_I}{G}\frac{\sqrt{r}}{\sqrt{2\pi}} \sin\frac{\theta}{2}\left[M_4 - \cos^2\frac{\theta}{2}\right] \tag{7b}$$

where r and θ are the polar coordinates with the origin at the crack-tip, K_I is the mode I stress intensity factor and

$$M_3 = \begin{cases} \dfrac{1-\nu}{1+\nu} & \text{(plane stress)} \\ 1-2\nu & \text{(plane strain)} \end{cases} \tag{7c}$$

$$M_4 = \begin{cases} \dfrac{2}{1+\nu} & \text{(plane stress)} \\ 2-2\nu & \text{(plane strain)} \end{cases} \tag{7d}$$

After substituting Equations (7a) and (7b) into Equations (6a) and (6b), the first and second terms of the integrand in Equations (6a) and (6b) are evaluated along a non-dimensionalized half square contour, 01234, as shown in Figure 2. Results of the numerical integration using either the first and second terms or the first term alone in Equations (6a) and (6b) as one traverses along the half contour are plotted in Figures 2 and 3. In these figures, the former and latter J-integral values are denoted as "theoretical" and "approximate" values respectively. Notable is the close proximity between the theoretical and approximate summation of ΔJ, $\Sigma\Delta J$, along the contour before entering segment 34. The nondimensionalized $J=\Sigma\Delta J$ values at point 4 shows about 14% difference between the theoretical and approximate $\Sigma\Delta J$ values.

We further evaluate the validity of this J approximation procedure for a crack tip region characterized by a Hutchinson-Rice-Rosengren singular field [27,28]. Again consider a rectangular contour surrounding a crack tip as shown in the legend of Figure 4. The HRR stress, strain and displacement field within this rectangular region can be expressed as [27,28]

$$\sigma_{ij} = \sigma_o \left[\frac{J}{\alpha\, \sigma_o \varepsilon_o I_N\, r} \right]^{\frac{1}{N+1}} \tilde{\sigma}_{ij}(\theta) \tag{8a}$$

$$\varepsilon_{ij} = \alpha\varepsilon_o \left[\frac{J}{\alpha\, \sigma_o \varepsilon_o I_N\, r} \right]^{\frac{N}{N+1}} \tilde{\varepsilon}_{ij}(\theta) \tag{8b}$$

$$u_i = \alpha\varepsilon_o r \left[\frac{J}{\alpha\, \sigma_o \varepsilon_o I_N\, r} \right]^{\frac{N}{N+1}} \tilde{u}_i(\theta) \tag{8c}$$

$$W = \frac{N}{N+1}\, \sigma_{ij}\, \varepsilon_{ij} \tag{8d}$$

where I_N is a dimensionless constant which varies with plane stress or plane strain conditions. $\tilde{\sigma}_{ij}(\theta)$, $\tilde{\varepsilon}_{ij}(\theta)$ and $\tilde{u}_i(\theta)$ are dimensionless functions

of θ. For the approximate J_h and J_v as represented by Equations (3) and (4), the needed σ_{yy} and W can be represented as

$$\sigma_{yy} = \sigma_o \left(\frac{\varepsilon_{yy}}{\alpha\, \varepsilon_o}\right)^{1/N} \tag{9a}$$

$$W = \frac{N}{N+1} \alpha\, \sigma_{yy}\, \varepsilon_{yy} \tag{9b}$$

Equation (9a) and (9b) represents the plastic components of Equations (2c) and (2d) where the elastic components are assumed negligible in the region characterized by the HRR field.

The approximate J can then be evaluated by substituting Equations (8a) and (8b) into Equation (9) and evaluating the integral along the non-dimensionalized half square contour. Also, the theoretical J is evaluated by substituting Equation (8) into Equation (1) and evaluating the integral along the non-dimensionalized half square contour. A state of plane stress with N=2, 5, 50 were chosen for this analysis. Numerical values for $\tilde{\sigma}_{ij}(\theta)$, $\tilde{\varepsilon}_{ij}(\theta)$ and $\tilde{u}_i(\theta)$ were obtained from [29]. The results are shown in Figures 4, 5 and 6. Good agreement between the theoretical and approximate J-integral are noted.

The results of Figures 2 through 6 suggest that the approximate J as determined by the far-field solution, is reasonably correct when used in a HRR dominated crack tip region. However, when used in a crack tip field dominated by linear elasticity, the error is noticeable. Figures 2 and 3 show that this error is generated during the last integration path or along the vertical contour, line 34, indicating that the assumed uniaxial tension state is not a reasonable approximation of the true state of elastic stresses along line 34. In contrast, both the assumed uniaxial tension state of stress and the true state of stresses of the HRR field along line 34 have negligible effect on the

J value as evidenced in Figures 4, 5 and 6 with the flat portion along the last integration path or line 34, and thus the approximate procedure of evaluating J works reasonably well. This induced error in the elastic crack tip stress field can be reduced if line 34 is situated within the region of uniaxial tension or more specifically along a free boundary. As will be shown later, under such restriction the approximate J will provide reasonably accurate J values in an elastic fracture specimen.

The J value can also be linked to the crack tip opening displacement (CTOD) through [30] as

$$\delta_t = D_N J/\sigma_o \tag{10}$$

where D_N values can be found in [29].

(2)Dugdale-Barenblatt Strip Yield Model

For an elastic perfect-plastic material, the crack-tip displacement fields for a Mode I plane stress Dugdale-Barenblatt strip yield model can be expressed [31] as

$$u_x = \frac{1}{2G}\frac{\sigma_o}{\pi}\left\{ 2\sqrt{rr_y}\cos\frac{\theta}{2}\left[1-2\nu+2\sin^2\frac{\theta}{2}\right] - (1-2\nu)r_y\Psi \right.$$
$$\left. -r[(1-2\sigma)(\Psi\cos\theta+\sin\theta\log R)-\sin\theta\log R]\right\}$$
$$+\frac{1}{2G}\sum_{n=1}^{\infty}\left\{(-1)^n d_{2n-1} r^{n-1/2}[F_1(n,\theta,\nu)\cos\theta - F_3(n,\theta,\nu)\sin\theta]\right.$$
$$\left. +(-1)^n d_{2n} r^n[-F_2(n,\theta,\nu)\cos\theta - F_4(n,\theta,\nu)\sin\theta]\right\} \tag{11a}$$

$$u_y = \frac{1}{2G}\frac{\sigma_o}{\pi}\left\{2\sqrt{rr_y}\sin\frac{\theta}{2}\left[2-2\nu-2\cos^2\frac{\theta}{2}\right]+(2-2\nu)r_y\log R\right.$$
$$\left. + r[(2-2\sigma)(\log R\cos\theta-\Psi\sin\theta)+\Psi\sin\theta]\right\}$$
$$+\frac{1}{2G}\sum_{n=1}^{\infty}\left\{(-1)^n d_{2n-1} r^{n-1/2}[F_1(n,\theta,\nu)\sin\theta + F_3(n,\theta,\nu)\cos\theta]\right.$$
$$\left. +(-1)^n d_{2n} r^n[-F_2(n,\theta,\nu)\cos\theta + F_4(n,\theta,\nu)\sin\theta]\right\} \tag{11b}$$

where

$$r_y = \frac{\pi}{4}\ \frac{d_1^2}{\sigma_o^2} = \frac{\pi}{8}\ \frac{K_I^2}{\sigma_o^2} \tag{11c}$$

$$F_1(n,\theta,\nu) = \left(\frac{7}{2} - n - 4\nu\right)\cos\left(n - \frac{3}{2}\right)\theta + \left(n - \frac{3}{2}\right)\cos\left(n + \frac{3}{2}\right)\theta$$

$$F_2(n,\theta,\nu) = (3 - n - 4\nu)\cos(n-1)\theta + (n+1)\cos(n+1)\theta \tag{11d}$$

$$F_3(n,\theta,\nu) = \left(\frac{5}{2} + n - 4\nu\right)\sin\left(n - \frac{3}{2}\right)\theta - \left(n - \frac{3}{2}\right)\sin\left(n + \frac{1}{2}\right)\theta$$

$$F_4(n,\theta,\nu) = -(3+n-4\nu)\sin(n-1)\theta + (n+1)\sin(n+1)\theta$$

$$\Psi = \tan^{-1}\left\{\frac{-2\sqrt{r_y r}\cos\theta/2}{r_y - r}\right\}$$

$$R = \frac{[(r_y - r)^2 + 4r_y r\cos^2\theta/2\ )]^{1/2}}{r_y + r - 2\sqrt{r_y r}\sin\theta/2}$$

$$d_1 = \frac{K_I}{2\pi}$$

and K_I is the Mode I stress intensity factor.

The CTOD for the Dugdale-Barenblatt strip yield model become [31]

$$CTOD = \frac{1}{2G}(4-4\nu)\frac{\sigma_o}{\pi} r_y\left\{\frac{r}{r_y} - \left(\frac{r_y - r}{2\ r_y}\right)\log\left(\frac{r_y + r}{r_y - r}\right)\right\}$$
$$+\frac{1}{2G}\sum_{n=1}^{\infty}\left\{(-1)^{n+1} d_{2n-1} r^{n-1/2} F_3(n,\pi,\nu) + (-1) d_{2n} r^n F_2(n,\pi,\nu)\right\} \tag{12}$$

EXPERIMENTAL APPROACH

White light moire interferometry [32] was used to obtain a single-frame record of static and dynamic displacement fields surrounding the crack tip in slowly and rapidly fracturing 7075-T6 and 2024-0 aluminum SEN specimens. Figures 7 and 8 show the optical system which utilizes a compensator grating of half frequency, f/2, where f = 1200 lines/mm, to illuminate the reference and

specimen gratings of full and half frequencies, respectively. The achromatic light emerges from the compensator as monochromatic light beams at different diffraction angles and generates the same moire pattern for each wave length. The camera records the scalar sum of the light intensities associated with various wave length and thus much of the original white light intensity is recovered. When an incoherent light source is used, the gap between the reference and active gratings must be small. This white light moire interferometry provides the high sensitivity associated with high frequency gratings and the bright light source using a relatively simple experimental [illegible] white light moire fringe patterns were recorded on a 35 mm camera with [illegible] spatial filtering. A motor-driven camera provided up to 6 frames per second sequential records of the moire fringes. Using this [illegible] light source, which is used to align the optical system prior to recording, can be used to record dynamic moire fringe patterns [illegible] through rapidly discharge.

RESULTS

Fracture tests were conducted under monotonically increasing displacement loadings. The specimen configuration, material properties and the two material coefficients for the power hardening stress-strain relations are shown in Figure 9. These material properties indicate that aluminum 7075-T6 is essentially an elastic-perfect plastic material while 2024-T3 is a strain hardening material. Figures 10 and 11 are typical white light moire interferometry fringe patterns of aluminum 7075-T6 and 2024-0 CEN specimen with stable crack growth. The approximate J evaluation procedure was used to analyzed both 7075-T6 and 2024-T3 tests in plane stress along different paths which are shown in Figures 12 and 13.

7075-T6 SEN Specimens

Since 7075-T6 aluminum is a relatively brittle material with the crack-tip being surrounded with small scale yielding, the far-field J value as well as the near-field J value outside of the yield zone can be determined by elastic analysis. These elastic values are used to verify the accuracy of the experimental and data reduction procedures used in this paper.

Figure 12 shows the log-log plot of the u_y-displacement versus radial distance up to marked boundary where the slope was 0.5 ± 0.05. Experimental deviation in the slope of log u_y versus log r curve was determined by linear regression of a straight line fitting through the data points in Figure 12 and then computing the percentage deviation in slope from the crack tip. The average slope of 1/2 in the vicinity of the crack tip indicates that the elastic field prevailed in this specimen up to a distance 1.2 mm from the crack tip. The approximate J values which were determined by the above mentioned J evaluation procedure are shown in Table 1. Also shown for comparison purpose in Table 1 are the corresponding stress intensity factor values computed by $K = \sqrt{J^*E}$ using the J values obtained from the moire fringes and the K values computed by using the formula in ASTM STP 410 [33], the William s polynomial function [34] and the Dugdale strip yield model. Figure 13 is the corresponding plots of the stress intensity factor, K, versus applied load. Good agreements between the measured K and that computed by ASTM STP 410 results are noted. Also shown in Table 1 are the experimentally measured and the computed CTOD values based on the Dugdale-Barenblatt strip yield model. The computed CTOD value were obtained by least square fitting Equation (11) with n=2 which is a four parameter characterization of the crack tip stress field to the u_y-displacement field of the moire fringes. The

parameters, (e.g. d_n and r_y) were then back substituted to Equation (12) and the CTOD value was computed. Figure 14 shows CTOD plots of the 7075-T6 fatigue precracked specimens versus applied load. The same CTOD values were observed before the onset of unstable crack growth in this fatigue pre-cracked SEN specimens.

Table 2 shows the approximate J values which were determined along the three contours in the 7075-T6 SEN specimen shown in Figure 10, for ten sequential moire fringe patterns of stable crack growth. As expected in this elastic specimen, the J-values along these three contours, far to near field contours are in good agreement with each other.

2024-0 SEN Specimens

A 2024-0 SEN specimens, with fatigue precrack, were tested to failure. Unlike the 7075-T6 specimens, no unstable crack growth were observed in these specimens which exhibited large scale yielding. Figure 15 shows the log-log plots of the u_y-displacement versus distance to the crack tip of Figure 11. The average slopes near the crack tip within the marked region in Figure 15 is $1/6 \pm 0.02$ which is the predicted exponent for a HRR displacement fields [27,28]. Table 3 shows the approximate J values obtained from the sequential moire interferometry recordings of the test specimen along three different paths as shown in Figure 11 for each frame. These results show that within the relatively short crack extension of 0.75 mm, J is still a valid parameter for characterizing the crack tip [35] and Equation (10) is valid within this loading range. The path independency of the measured J values for each frame is an experimental validation of the J estimation procedure proposed in this paper. Figure 16 shows the increases in the approximate J values, which are consistent with published results [20,21], with crack extension for

the 2024-O specimen. Notable in Figure 16 is the slopes dJ/da of the J values which remain constant during the initial short crack extension of 0.4-0.5 mm and its continuous decrease beyond this short crack extension. Figure 17 shows the increases in CTOD values with crack extension. These CTOD values can be linked to the corresponding measured J values through Equation (10) where Figure 18 show the variations of the experimental determined D_N values which agree favorably with the D_N value determined by the HRR field, (e.g., D_N=0.33 for 2024-0 aluminum material).

CONCLUSIONS

1. White light moire technique was used to determine the u_y-displacement field of stably growing cracks in 7075-T6 and 2024-0 aluminum SEN specimens.
2. An procedure for estimating J from the recorded u_y-displacement field was developed. This approximate J agrees reasonably well in a HRR crack tip field but required special handling when used in an elastic crack tip field.
3. The approximate J and CTOD at the onset and during stable crack growth were recorded. Limited data suggests that there exist a constant CTOD for unstable crack propagation in 7075-T6 aluminum SEN specimen. HRR field dominates stable crack growth in 2024-0 aluminum SEN specimen.

ACKNOWLEDGMENT

The work reported here was completed under ONR Contract N00014-85-K-0187. The authors wish to acknowledge the support and encouragement of Dr. Yapa Rajapakse, ONR, during the course of this investigation.

REFERENCES

1. Kobayashi, A.S. and Lee, O.S., "Elastic Field Surrounding a Rapidly Tearing Crack," Elastic-Plastic Fracture, Vol. I, Inelastic Crack Analysis, ed. by C.F. Shih and J.P. Gudas, ASTM STP 803, pp. I-21-I-38, (1983).

2. Lee, O.S., Kobayashi, A.S. and Komine, A., "Further Studies on Crack Tip Plasticity of a Tearing Crack," Experimental Mechanics, Vol. 25, No. 1, pp. 66-74, (1985).

3. Emery, A.F., Kobayashi, A.S., Love, W.J., Place, B.H., Lee, ..H. and Chao, Y.H., "An Experimental and Analytical Investigation ot Axial Crack Propagation in Long Pipes," Engineering Fracture Mechanics, Vol. 23, pp. 215-228, (1986).

4. Rice, J.R., Drugan, W.J. and Sham, T.-L., "Elastic-Plastic Analysis of Growing Cracks," Fracture Mechanics: Twelfth Conference, ASTM STP 700, pp. 189-221, (1980).

5. Amazigo, J.C. and Hutchinson, J.Q., "Crack Tip Field in Steady Crack-Growth with Linear Strain-Hardening," Journal of the Mechanics and Physics of Solids, Vol. 25, pp. 81-97, (1977).

6. Gao, Y.-C. and Hwang, K.-C., "Elastic-Plastic Field in Steady Crack Growth in a Strain- Hardening Material," Advances in Fracture Mechanics, Proceedings, Fifth International Conference on Fracture, Cannes, France, pp. 669-682, (1981).

7. Rice, J.R., "Elastic-Plastic Crack Growth," Mechanics of Solids, edited by H.G. Hopkins and M.J. Sewell, Pergamon Press, Oxford, pp. 539- 562, (1982).

8. Gao Y.-C. and S. Nemat-Nasser, "Near-Tip Dynamic Fields for a Crack Advancing in a Power-Law Elastic-Plastic Material: Modes I, II and III," Mechanics of Material, Vol. 2, pp. 305-317, (1983).

9. Chitaley, A.D. and McClintock, F.A., "Elastic-Plastic Mechanics of Steady Crack Growth Under Anti-Plane Shear," Journal of the Mechanics and Physics of Solids, Vol. 19, pp. 147-163, (1971).

10. Sorensen, E.P., "A Numerical Investigation of Plane Strain Stable Crack Growth Under Small-Scale Yielding Conditions," Elastic-Plastic Fracture, ASTM STP 668, pp. 151-174, (1979).

11. Anderson, H., "Finite Element Treatment of A Uniformly Moving Elastic-Plastic Crack Tip," Journal of the Mechanics and Physics of Solids, Vol.22, pp. 285-308, (1974).

12. Dean, R.H. and Hutchinson, J.W., "Quasi-Static Steady Crack Growth in Small-Scale Yielding," Fracture Mechanics: Twelfth Conference, ASTM STP 700, pp. 383-405, (1981).

13. Dean, R.H., "Elastic-Plastic Steady Crack Growth in Plane Stress," Elastic-Plastic Fracture, Vol. I, Inelastic Crack Analysis, ed. by C.F. Shih and J.P. Gudas, ASTM STP 803, pp. 39-51, (1983).

14. Green, G. and Knott, J.F., "On Effects of Thickness on Ductile Crack Growth in Mild Steel," Journal of the Mechanics and Physics of Solids, Vol. 23, pp. 167-183, (1975).

15. de Koning, A.U., "A Contribution to the Analysis of Quasi-Static Crack Growth," Fracture 1977, Proceedings 4th International Conference on Fracture, University of Waterloo Press, Vol. 3, pp. 25-31, (1977).

16. Green, G. and Knott, J.F., "The Initiation and Propagation of Ductile Fracture in Low Strength Steels," Journal of Engineering Materials and Technology, Trans ASME, Series H 98, (1975).

17. McClintock, F.A. and Irwin, G.R., "Plasticity Aspects of Fracture Mechanics," Fracture Toughness Testing and Its Applications, ASTM STP 381, pp. 84-113, (1965).

18. Achenbach, J.D. and Dunayevsky, V., "Crack Growth Under Plane Stress Conditions in an Elastic Perfectly-Plastic Material," Journal of the Mechanics and Physics of Solids, Vol. 32, No. 2, pp. 89-100, (1984).

19. Broberg, K.B., "On Stable Crack Growth," Journal of the Mechanics and Physics of Solids, Vol. 23, pp. 215-237, (1975).

20. Kanninen, M.F. Rybicki, E.F., Stonesifer, R.B., Broek, D., Rosenfield, A.R., Marschall, C.W., and Hahn, G.T., "Elastic-Plastic Fracture Mechanics for Two-Dimensional Stable Crack Growth and Instability Problems," Elastic-Plastic Fracture, ASTM STP 668, pp. 121-150, (1979).

21. Shih, C.F., deLorenzi, H.G., and Andrew, W.R., "Studies on Crack Initiation and Stable Crack Growth," Elastic-Plastic Fracture, ASTM STP 668, pp.65-120, (1979).

22. Paris, P.C. Tada, H. Zahoor, A. and Ernst, H., "The Theory of Instability of the Tearing Mode of Elastic-Plastic Crack Growth," Elastic-Plastic Fracture, ASTM STP 668, pp. 5-36, (1979).

23. Rice, J.R., "A Path Independent Integral and the Approximate Analysis of Strain Concentration by Notches and Cracks," Journal of Applied Mechanics, pp. 379-386, (1968).

24. King, R.B. and Herrmann, G., "Nondestructive Evaluation of the J and M Integrals," Journal of Applied Mechanics, Vol. 48, pp. 83-87, (1981).

25. Read, D.T. and McHenry, H.I., "Strain Dependence of the J-Contour Integral in Tensile Panels," Advance in Fracture Research, edited by D. Francois et al, (1980).

26. Read, D.T., "Experimental Method for Direct Evaluation of the J Contour Integral," ASTM STP 791, pp. 199-213, (1983).

27. Hutchinson, J.W., "Singular Behavior at the End of Tensile Crack in a Hardening Material," Journal of Mechanics and Physics of Solids, Vol. 16, pp. 13-31, (1968).

28. Rice, J.R. and Rosengren, G.F., "Plane Strain Deformation near a Crack Tip in a Power-Law Hardening Material," Journal of Mechanics and Physics of Solids, Vol. 16, pp. 1-12, (1968).

29. Shih, C.F., "Tables of Hutchinson-Rice-Rosengren Singular Field Quantities," MRL E-147, Materials Research Laboratory, Brown University, (1983).

30. Tracy, D.M., "Finite Element Solutions for Crack Tip Behavior in Small-Scale Yielding," Journal of Engineering Materials and Technology, Vol. 98, pp. 146-151, (1976).

31. Kang, B.S.-J., Kobayashi, A.S., and Post, D., "Stable and Rapid Crack Propagation in Aluminum Tensile Specimens," Proceedings of the 1985 SEM Spring Conference on Experimental Mechanics, Las Vegas, pp. 9-12, (1985).

32. Post, D. "Moire Interferometry with White Light," Applied Optics, Vol. 18, No. 24, pp. 4163-4167, (1979).

33. "Plane Strain Crack Toughness Testing of High Strength Metallic Materials," American Society for Testing and Materials, ASTM STP 410, pp. 12 (1966).

34. Williams, M.L., "On the Stress Distribution at the Base of a Stationary Crack," Journal of Applied Mechanics, Vol. 24, pp. 109-114, (1957).

35. Hutchinson, J.W. and Paris, P.C., " Stability Analysis of J-Controlled Crack Growth." Elastic-Plastic Fracture, ASTM STP 668, pp. 37-64, (1979).

Table 1 Measured and Calculated J, K and CTOD of 7075-T6 Aluminum SEN Specimen with Fatigue Precrack.

Frame no.	Applied load (KN)	Crack length (mm)	Measured J (MPa m)	K (stress intensity factor) 1* (MPa $\sqrt{m}$)	2*	3*	4*	Measured CTOD (10^{-3}mm)	Calculated CTOD ** (10^{-3}mm)
1	1.17	2.18	0.0008	7.7	7.5	7.8	7.7	3.3	4.1
2	1.93	2.18	0.0022	12.1	12.5	14.7	13.0	4.1	5.0
3	2.85	2.18	0.0050	18.8	18.9	20.5	16.9	5.8	7.9
4	3.30	2.40	0.0066	23.1	21.8	22.2	21.8	7.3	9.5
5	3.60	2.48	0.0083	25.9	24.4	27.6	22.8	7.9	10.1
6	3.98	2.65	0.0110	29.9	28.1	28.2	25.7	9.1	11.2
7	4.29	2.84	0.0133	33.9	30.8	29.4	28.6	9.9	14.1
8***	4.35	2.94	0.0151	35.2	32.9	30.0	28.9	9.9	15.0
9***	4.61	3.11	0.0205	38.9	38.3	37.9	32.2	9.9	18.0
10***	4.90	4.01	0.0340	50.8	49.1	43.3	37.6	9.9	20.2

1* : based on ASTM STP 410 K evaluation procedure.
2* : based on J evaluation procedure, e.g. $K=\sqrt{J*E}$.
3* : based on the William's polynomial function.
4* : based on the Dugdale-Barenblatt strip yield model.
** : based on the Dugdale-Barenblatt strip yield model.
***: rapid crack growth.

Table 2 Measured Approximate J Values for Different Contours in 7075-T6 Aluminum SEN Specimen with Fatigued Precrack.

Frame no.	Applied load (KN)	Crack length (mm)	Measured J #1 (Mpa m)	#2 (Mpa m)	#3* (Mpa m)
1	1.17	2.18	0.75×10^{-3}	0.79×10^{-3}	0.81×10^{-3}
2	1.93	2.18	1.96×10^{-3}	2.15×10^{-3}	2.43×10^{-3}
3	2.85	2.18	4.66×10^{-3}	5.03×10^{-3}	5.23×10^{-3}
4	3.30	2.40	6.32×10^{-3}	6.68×10^{-3}	7.00×10^{-3}
5	3.60	2.48	7.75×10^{-3}	8.36×10^{-3}	8.80×10^{-3}
6	3.98	2.65	10.7×10^{-3}	10.8×10^{-3}	11.6×10^{-3}
7	4.29	2.84	13.2×10^{-3}	13.3×10^{-3}	13.3×10^{-3}
8**	4.35	2.94	14.9×10^{-3}	15.1×10^{-3}	15.3×10^{-3}
9**	4.61	3.11	18.7×10^{-3}	20.4×10^{-3}	22.2×10^{-3}
10**	4.90	4.01	33.0×10^{-3}	33.7×10^{-3}	34.1×10^{-3}

* : far-field contour
**: rapid crack growth

Table 3 Measured Approximate J Values for Different Contours in 2024-O Aluminum SEN Specimen with Fatigued Precrack.

Frame no.	Applied load (KN)	Crack length (mm)	Measured J #1 (Mpa m)	#2 (Mpa m)	#3* (Mpa m)
1	0.90	1.59	0.37×10^{-3}	0.36×10^{-3}	0.36×10^{-3}
2	1.24	1.63	2.06×10^{-3}	2.03×10^{-3}	2.04×10^{-3}
3	1.46	1.66	3.30×10^{-3}	3.28×10^{-3}	3.27×10^{-3}
4	1.68	1.69	4.22×10^{-3}	4.17×10^{-3}	4.18×10^{-3}
5	1.81	1.74	6.23×10^{-3}	6.12×10^{-3}	6.10×10^{-3}
6	2.00	1.78	7.01×10^{-3}	6.71×10^{-3}	6.82×10^{-3}
7	2.11	1.89	10.2×10^{-3}	10.1×10^{-3}	10.0×10^{-3}
8	2.21	1.98	12.0×10^{-3}	11.6×10^{-3}	11.7×10^{-3}
9	2.23	2.14		13.2×10^{-3}	12.9×10^{-3}
10	2.30	2.36		14.8×10^{-3}	14.4×10^{-3}

* : far-field contour

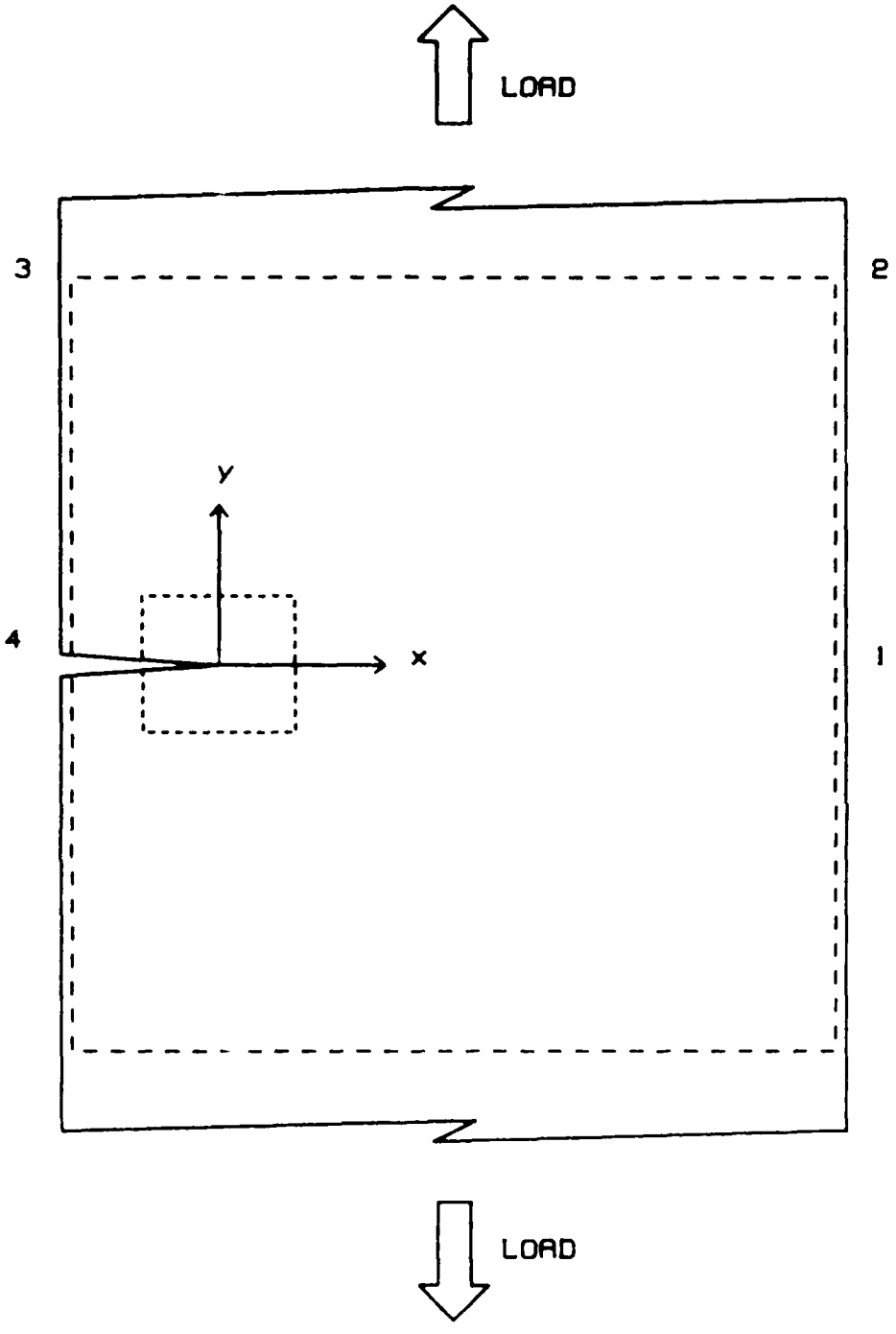

Figure 1. Contours for Direct Evaluation of Far and Near Field J-Integrals at a Single Edge Notched (SEN) Specimen.

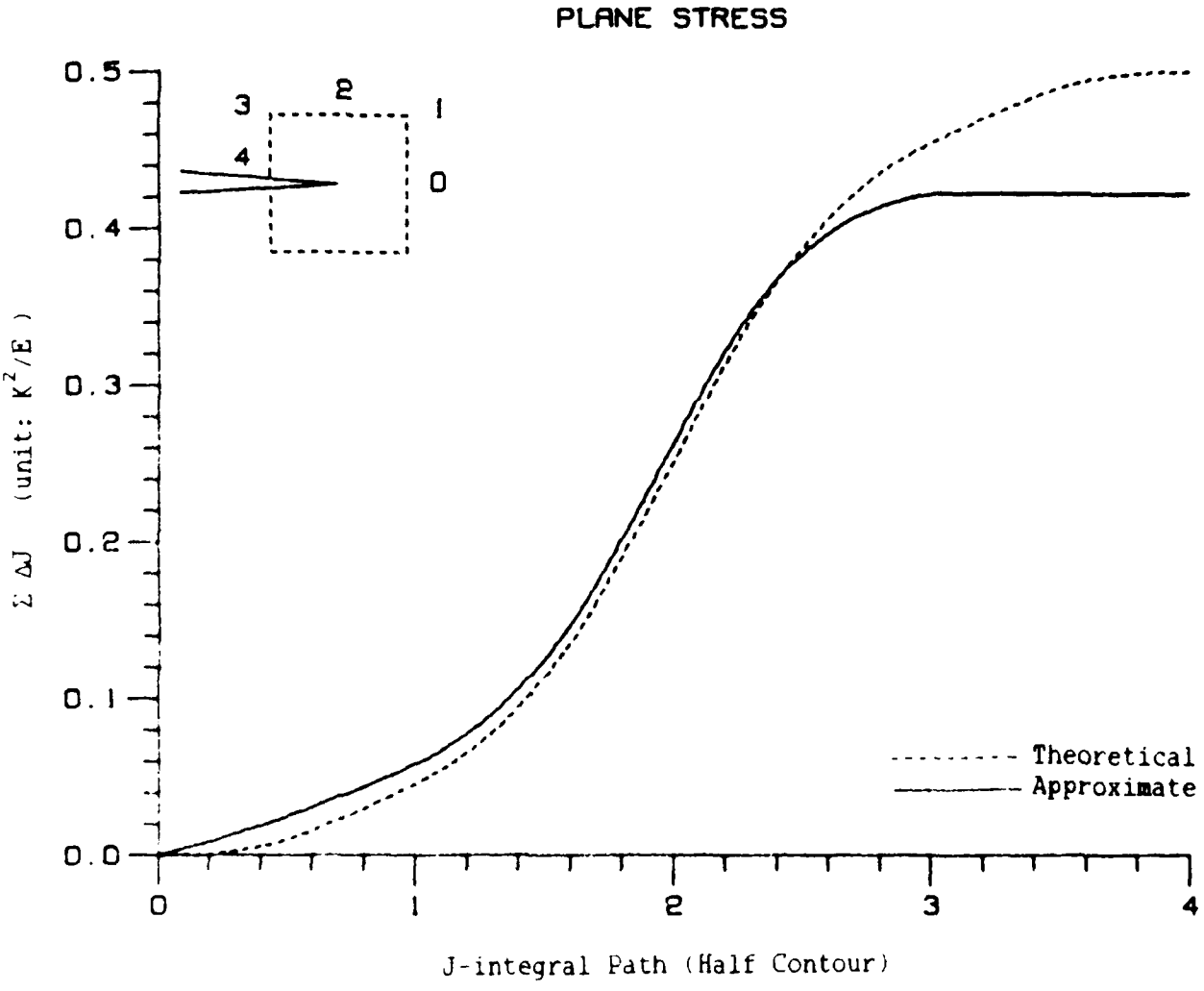

Figure Theoretical and Approximate Integral Values, $\Sigma\Delta J$. Linear Elastic, Plane Stress, $\nu=0.3$.

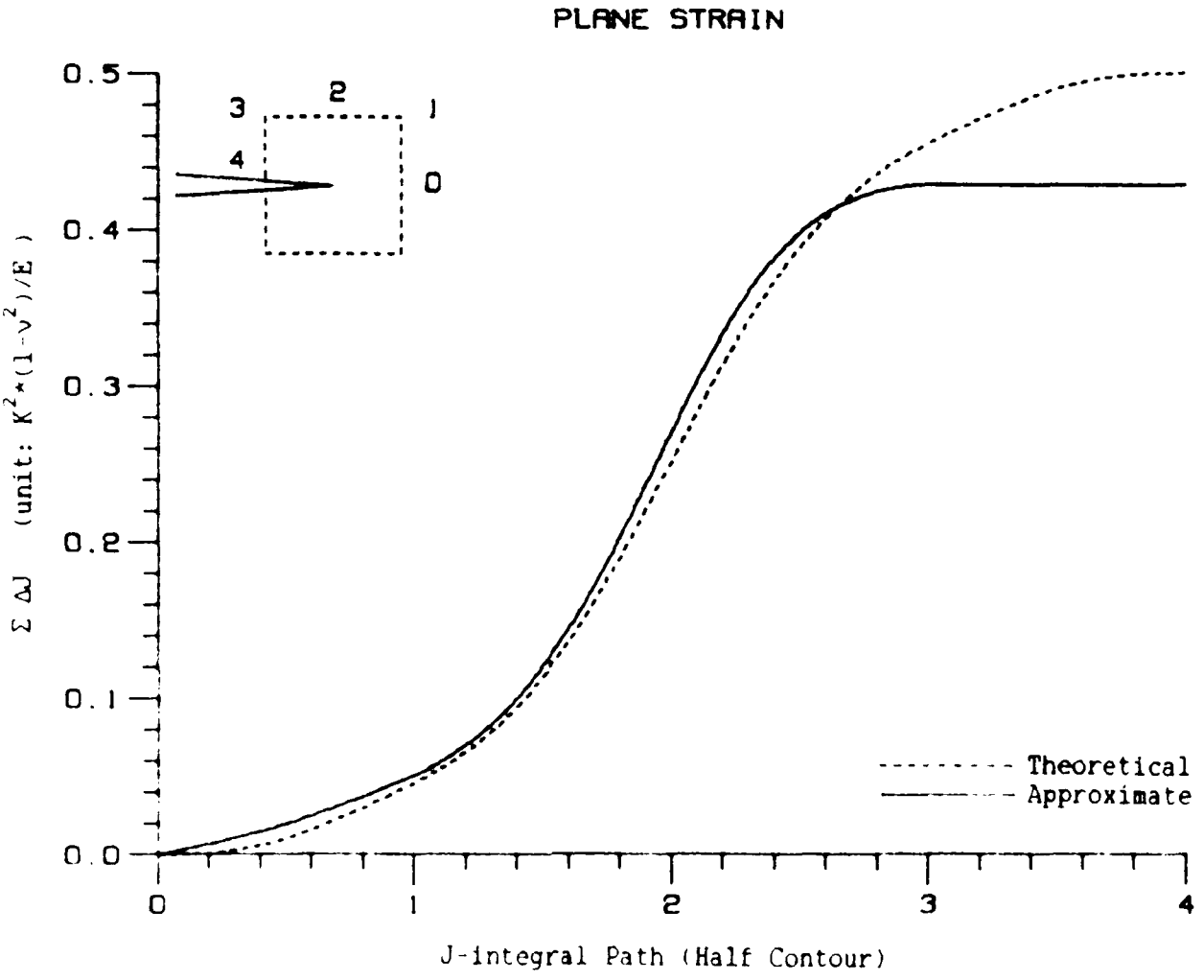

Figure 3. Theoretical and Approximate Integral Values, J3, Linear Elastic, Plane Strain, ν=0.3.

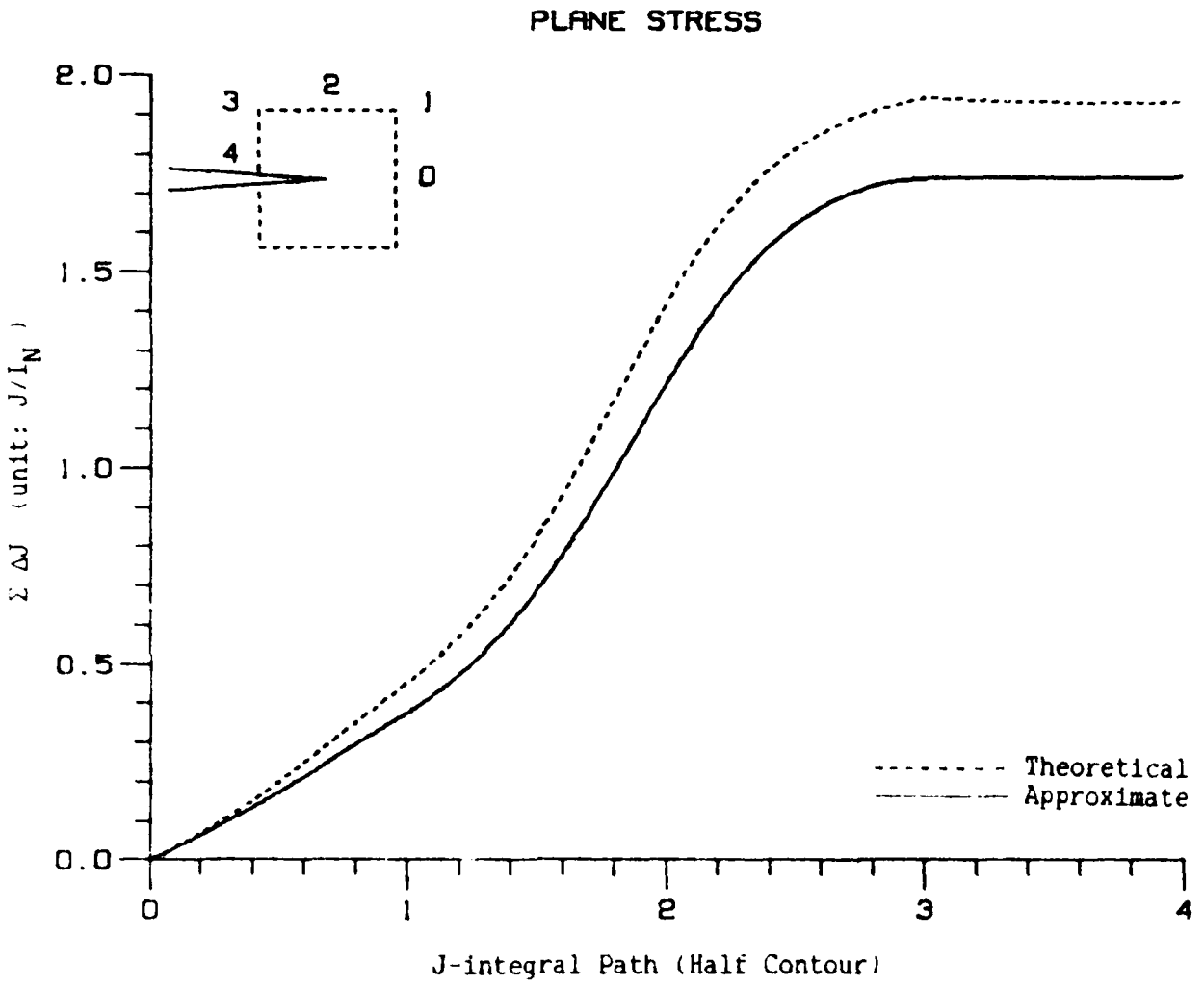

Figure 4 Theoretical and Approximate Integral Values, $\Sigma\Delta J$, Plane Stress HRR Field with N=2.

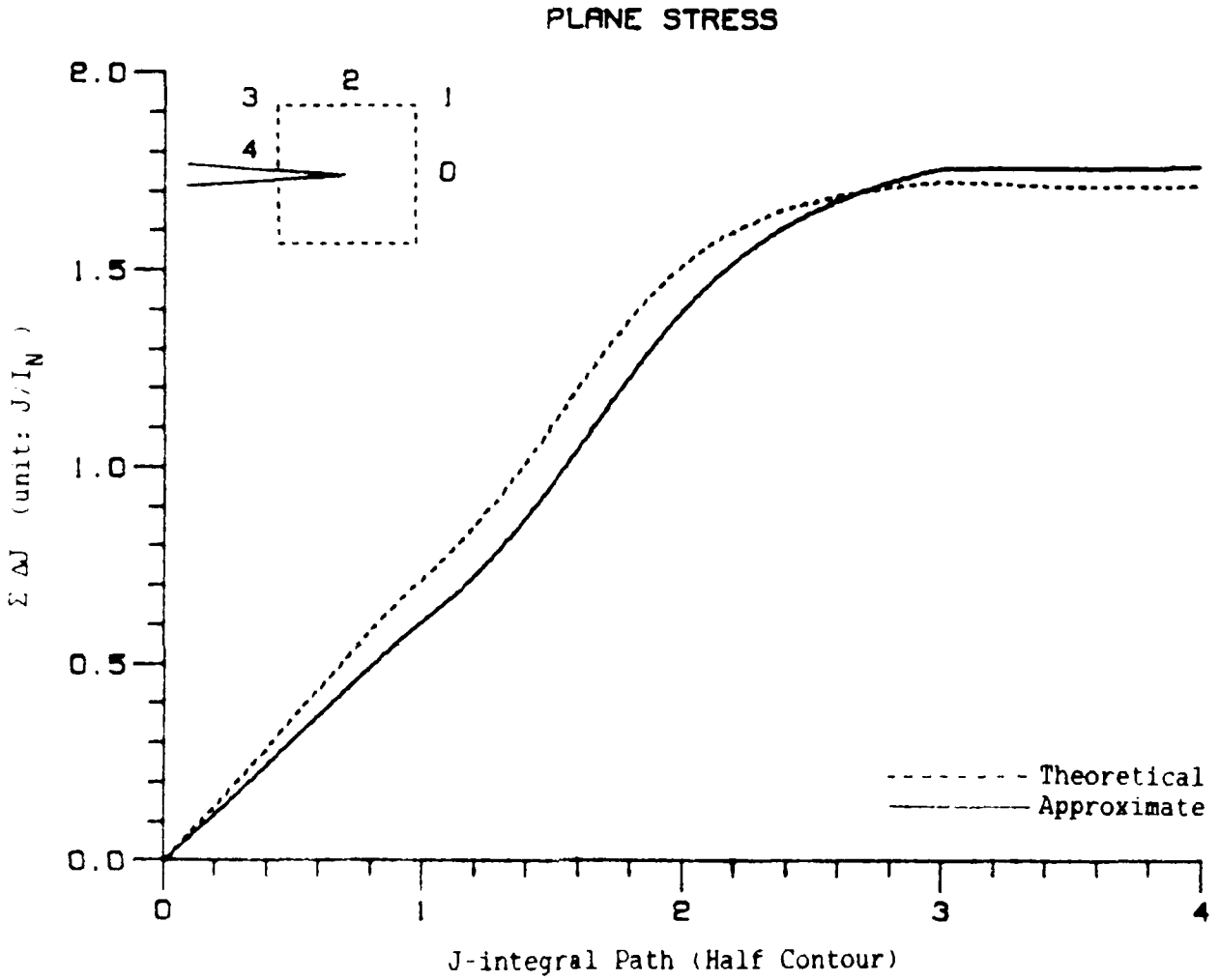

Figure 5 Theoretical and Approximate Integral Values, ΣΔJ, Plane Stress HRR Field with N=5.

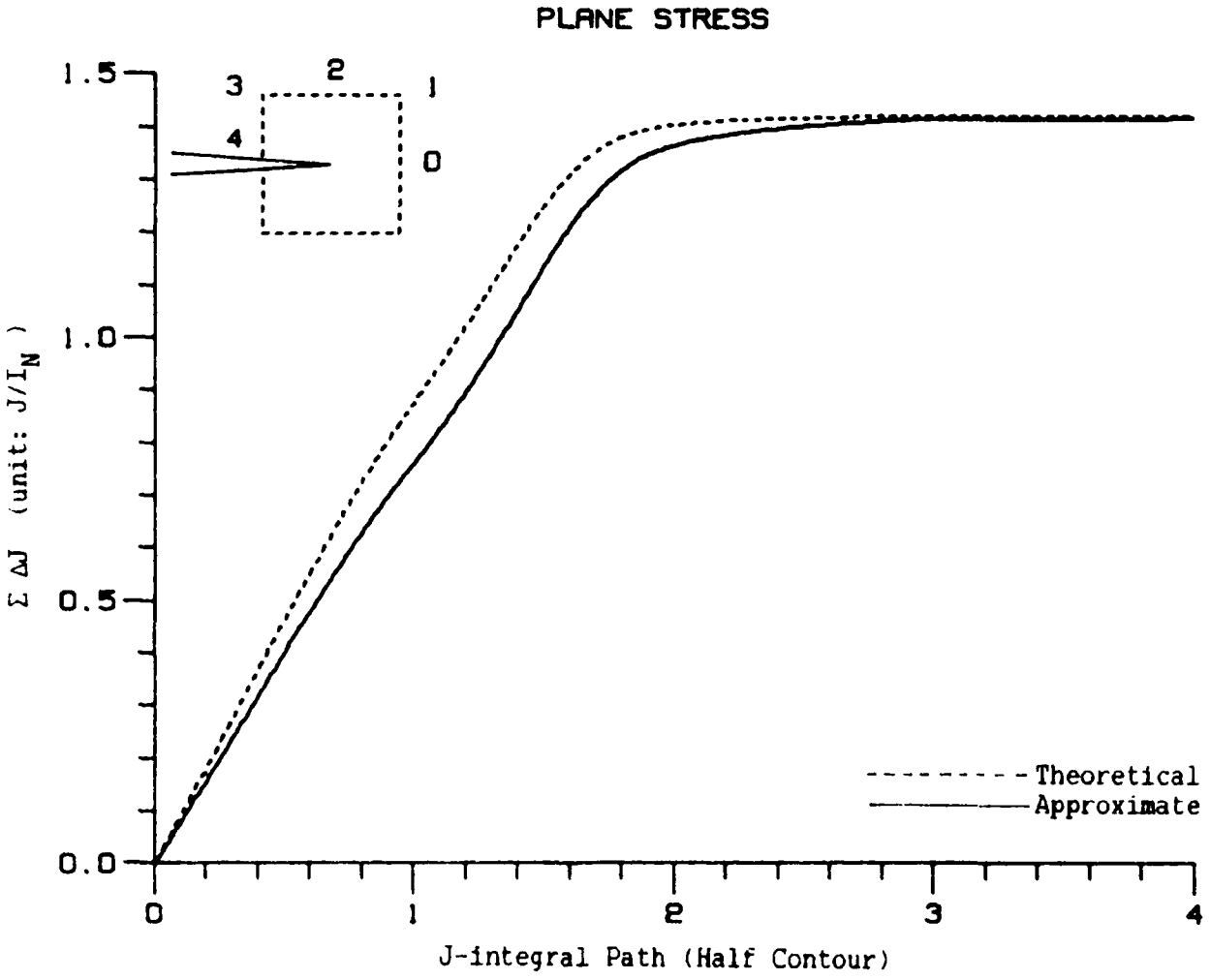

Figure 6 Theoretical and Approximate Integral Values, $\Sigma\Delta J$. Plane Stress HRR Field with N=50.

$$\sin \alpha = \frac{1}{2} \lambda f$$

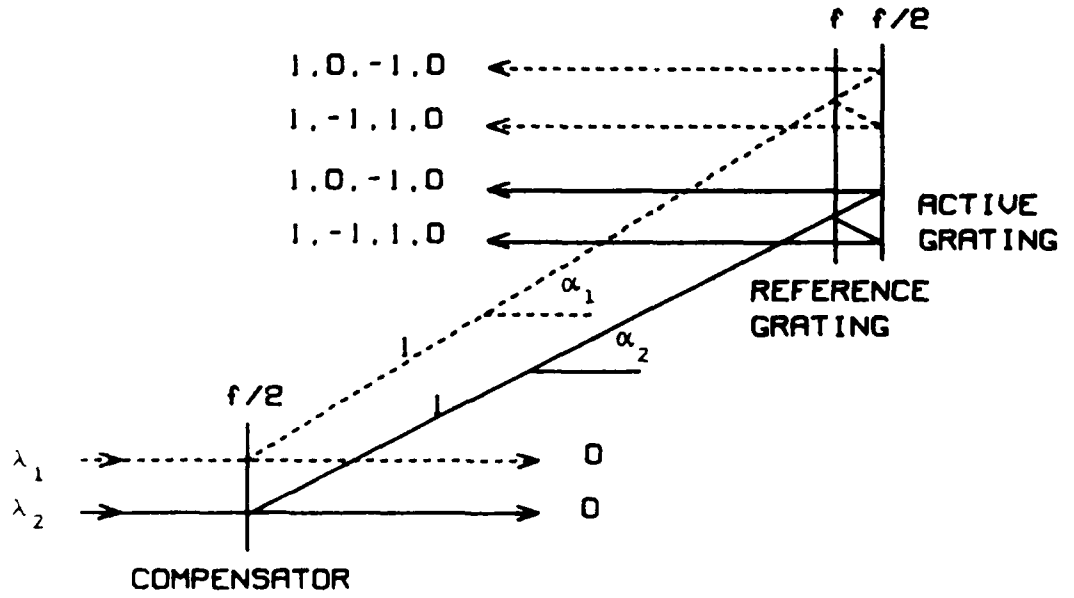

Figure 7 Optical Paths for White Light Moire Interferometry. (f=1200 lines/mm)

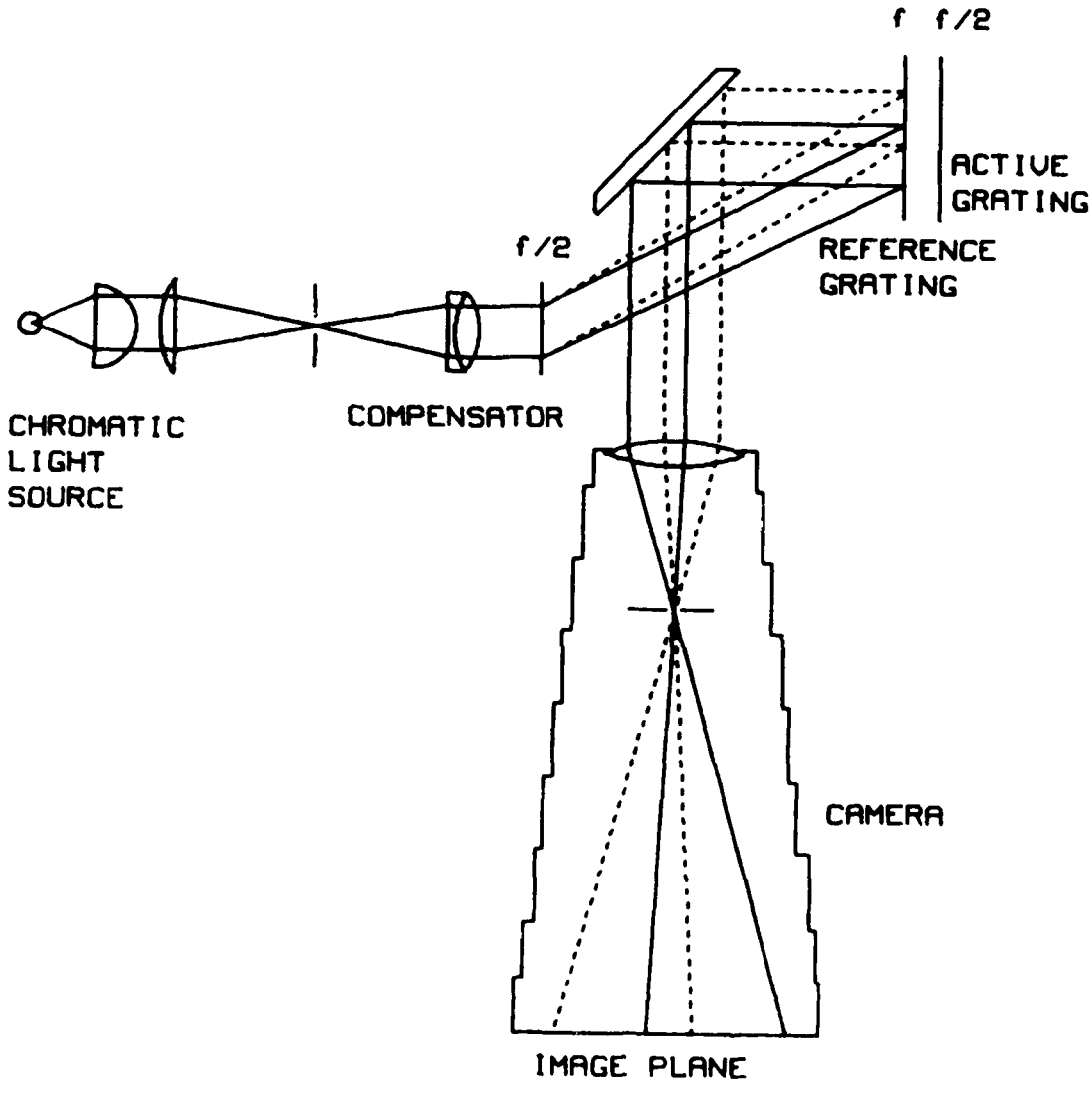

Figure 8 Optical Set-Up for White Light Moire Interferometry.
(f=1200 lines/mm)

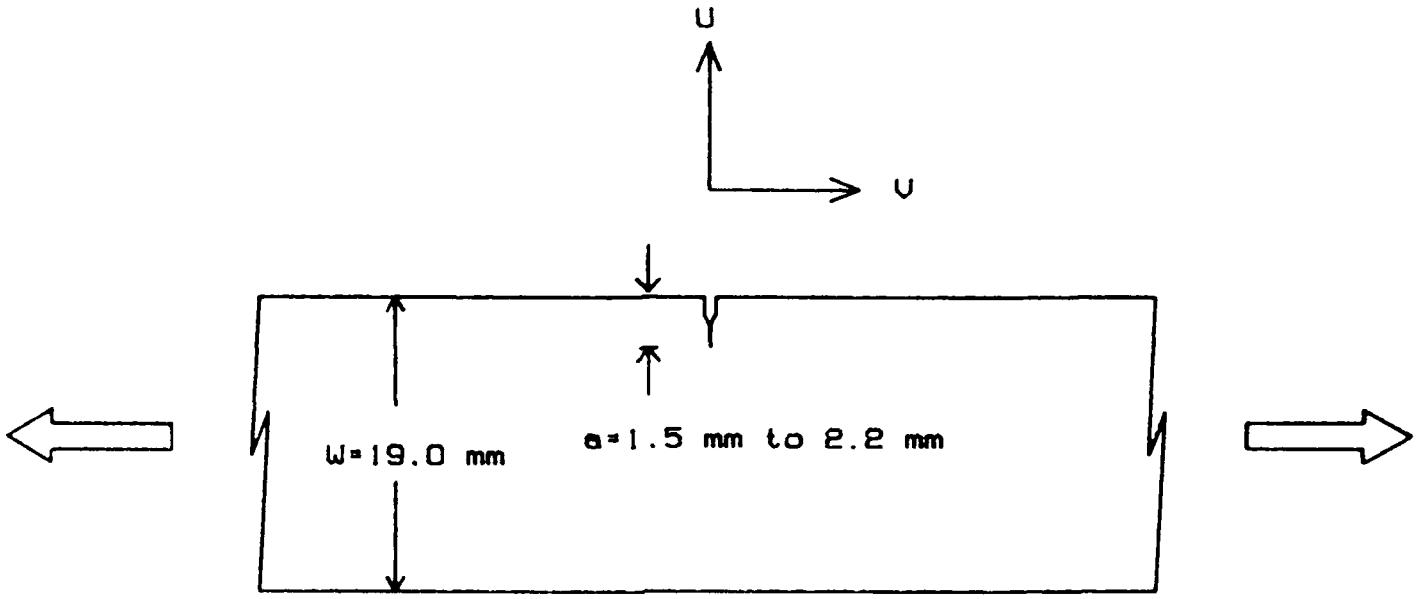

Specimen thickness: 0.8 mm

Aluminum	Yield Stress (MPa)	Young's Modulus (MPa)	α	N
2024-0	64	72260	0.35	5
7075-T6	504	71840	0.1	47

$$\varepsilon_{yy} = \frac{\sigma_{yy}}{E} + \alpha \frac{\sigma_{yy}}{E} \left(\frac{\sigma_{yy}}{\sigma_o} \right)^{N-1}$$

Figure 4. Single Edge Notched (SEN) Specimens.

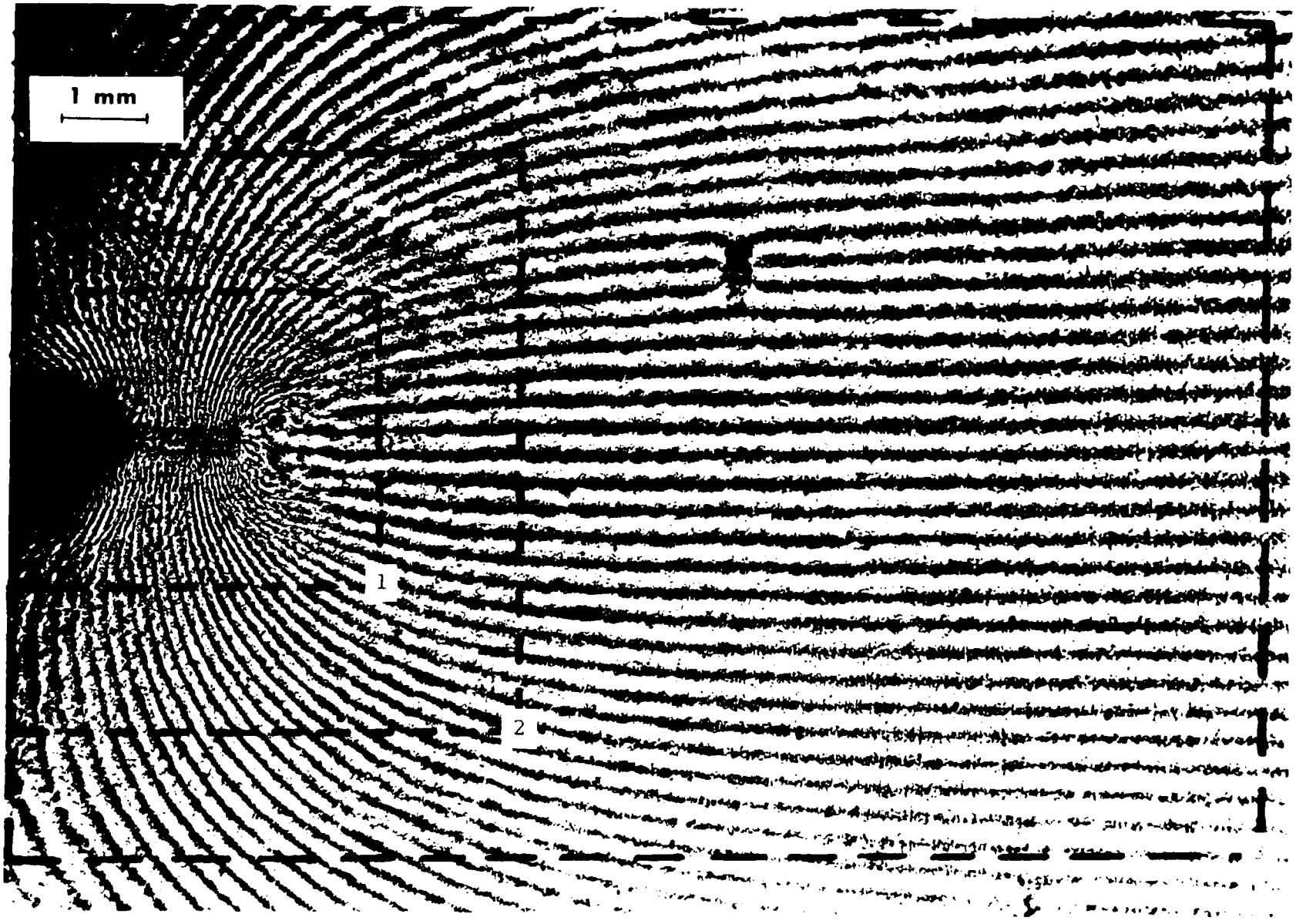

Figure 10 U_y-displacement Field Surrounding a Stably Extended Crack in a Fatigue Precracked 7075-T6 Aluminum SEN Specimen and the Paths Chosen for J-integral. Frame No. KJA1-3.

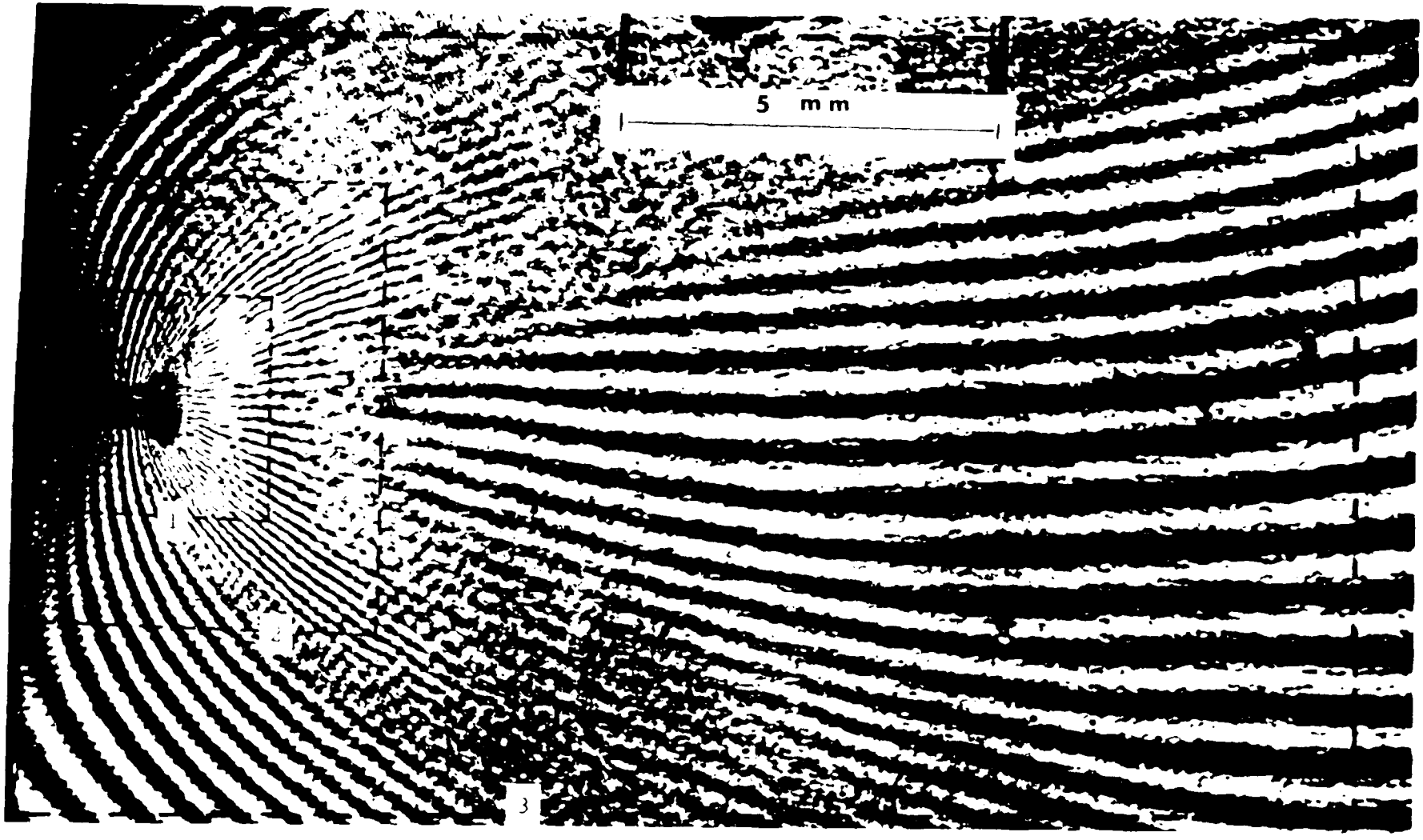

Figure 11 U_y displacement Field Surrounding a Stably Extended Crack in a Fatigue Precracked 2024-T Aluminum SEN Specimen and the Paths Chosen for J Integral. Frame No. KJC1 ..

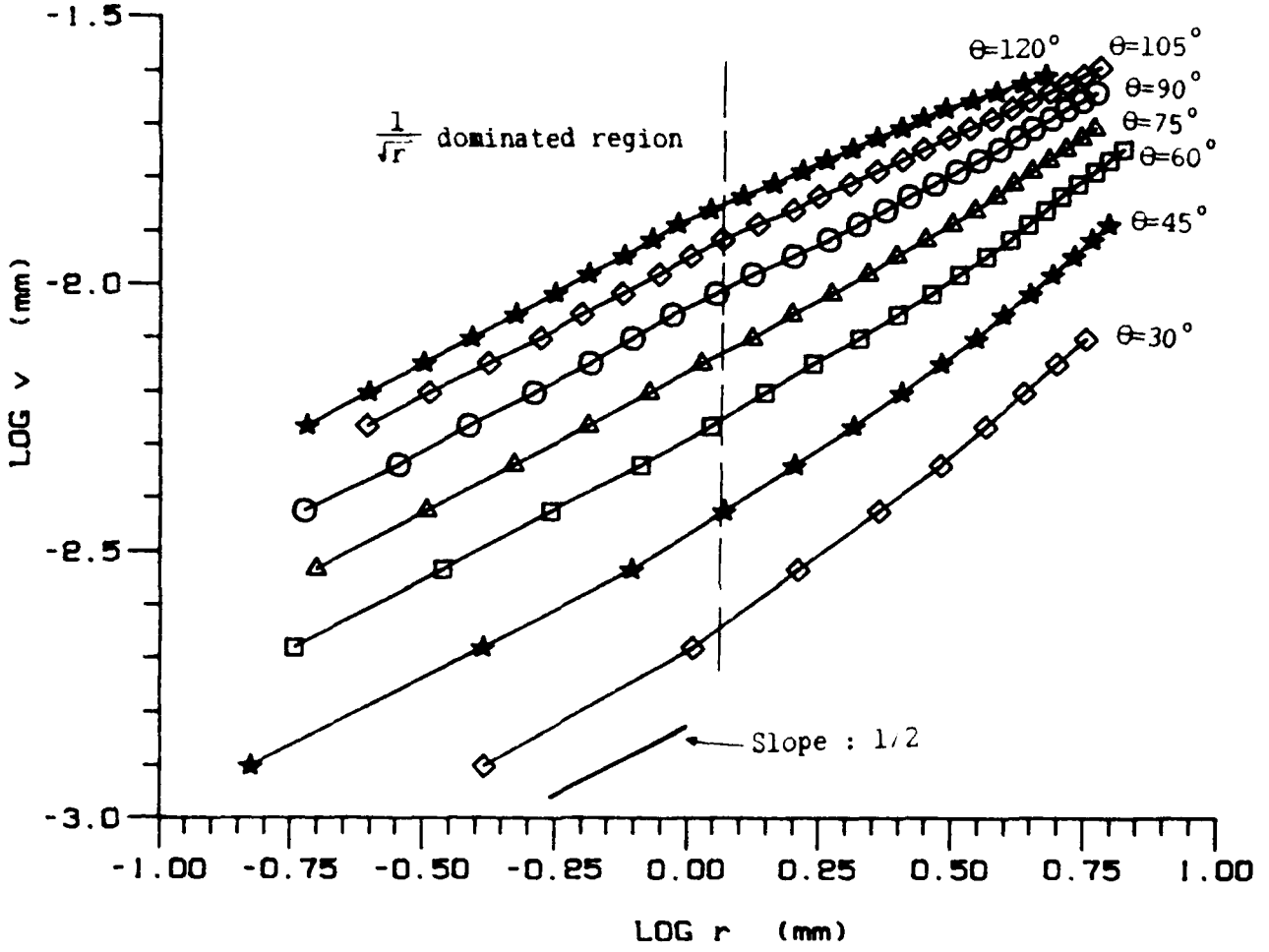

Figure 12 Log u_y Versus Log r Plots of U_y displacement Field. 7075-T6 Fatigue Precracked Aluminum SEN Specimen. Frame No. KJA1-3.

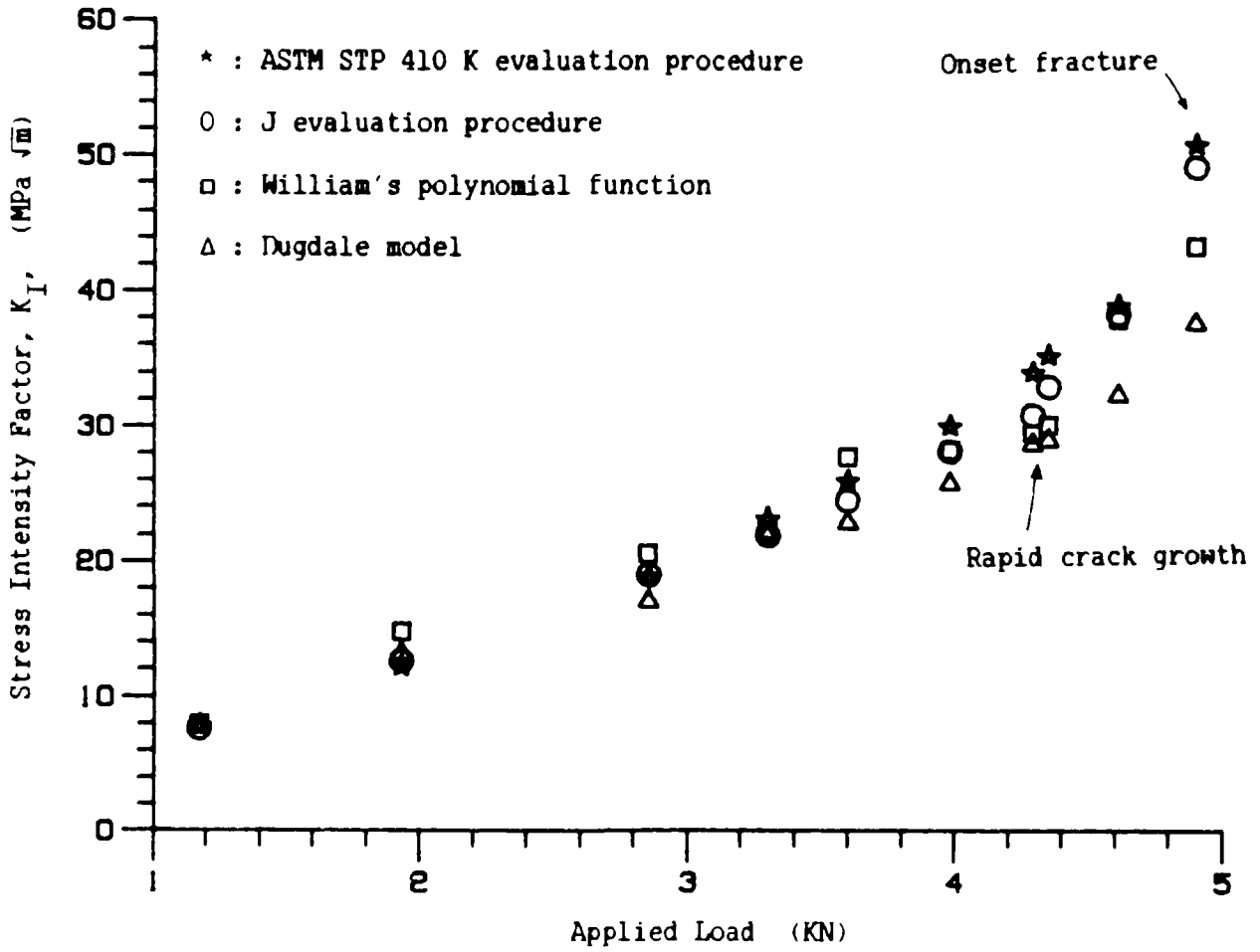

Figure 13 Stress Intensity Factor Versus Applied Load. 7075-T6 Aluminum Fatigue Precracked SEN Specimen. Specimen No. KJA1.

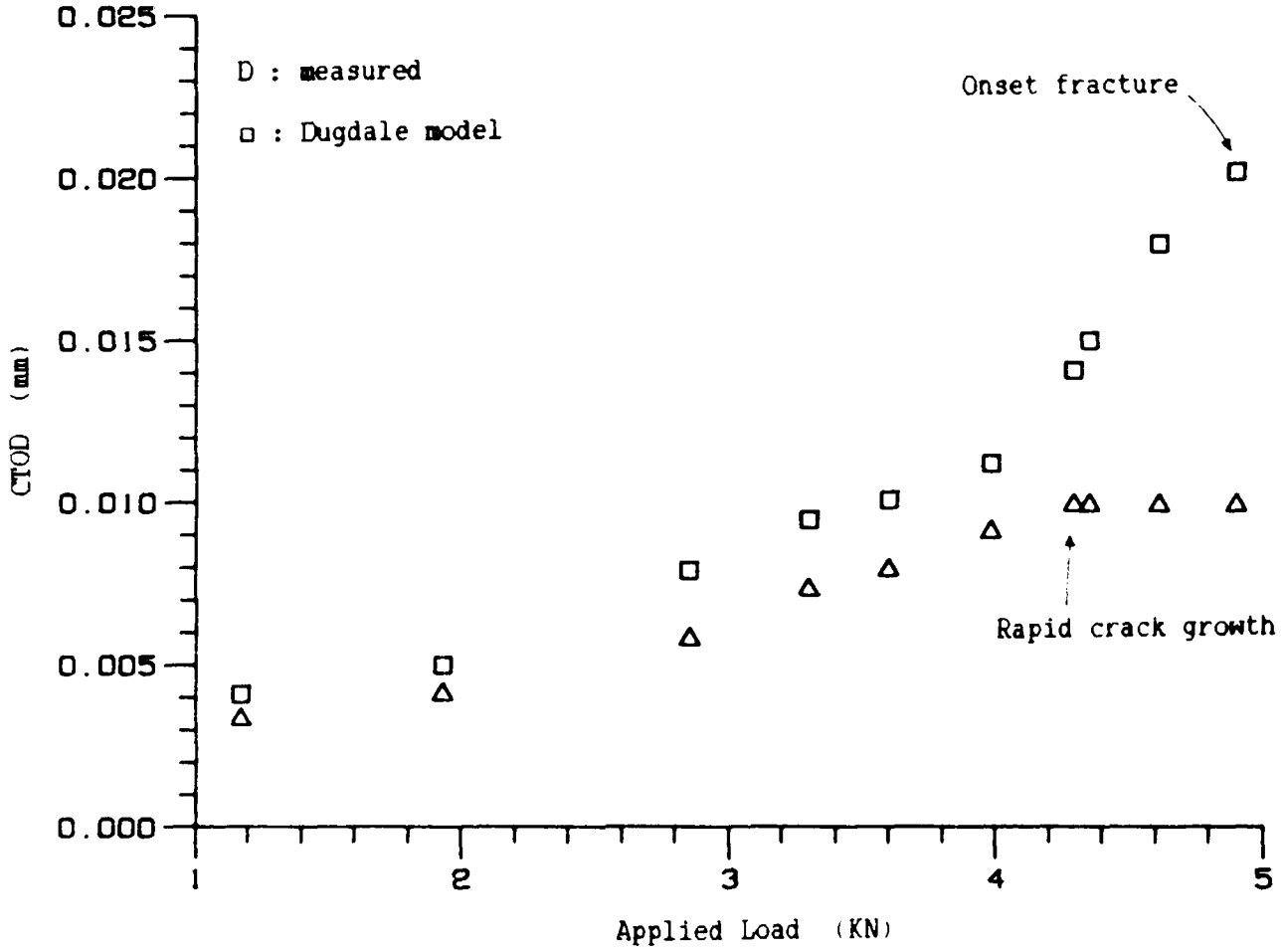

Figure 14 Crack Tip Opening Displacement Versus Applied Load. 7075-T6 Aluminum Fatigue Precracked SEN Specimen. Specimen No. KJA1.

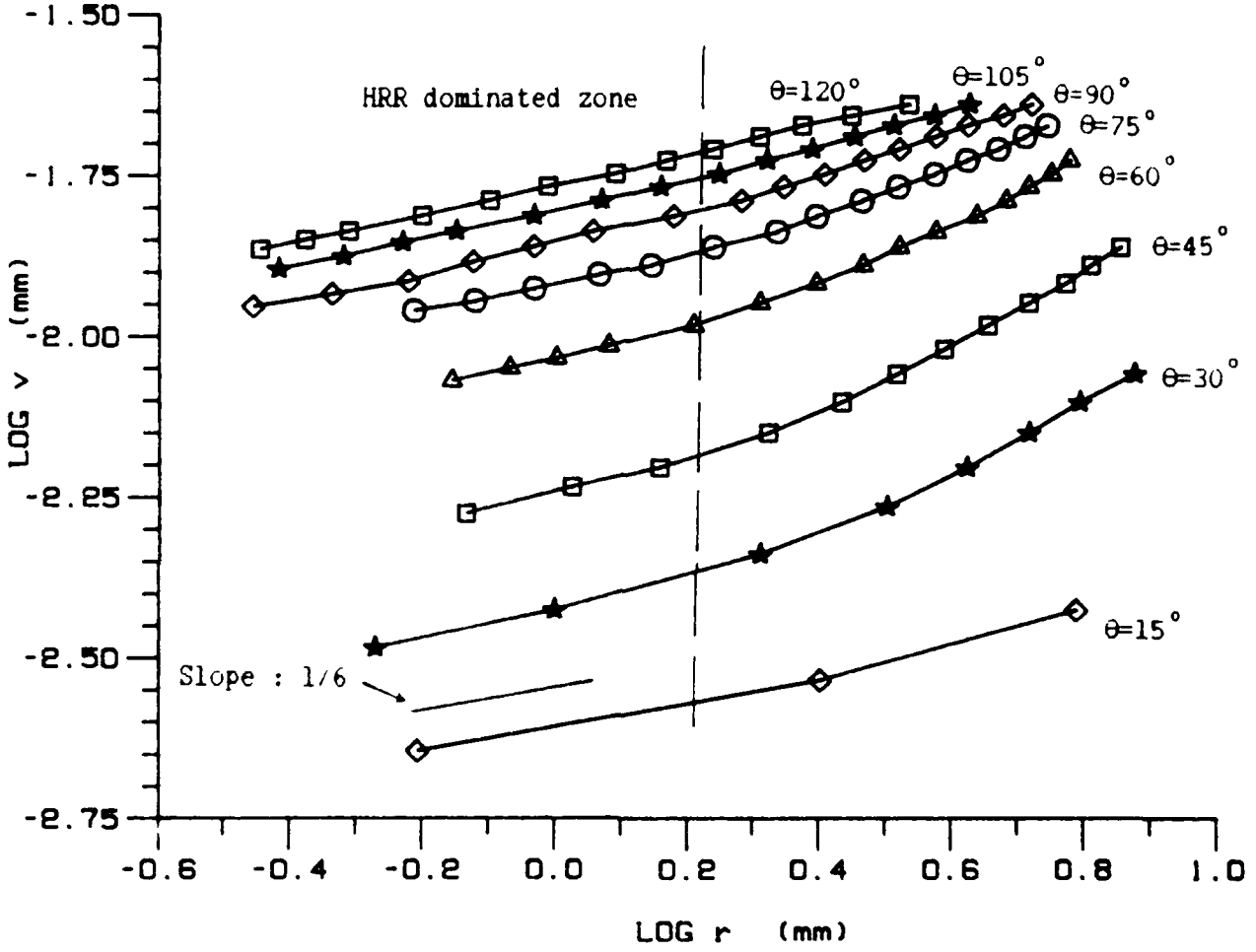

Figure 15 Log u_y Versus Log r Plots of U_y-displacement Field. 2024-0 Fatigue Precracked Aluminum SEN Specimen. Frame No. KJC1-2.

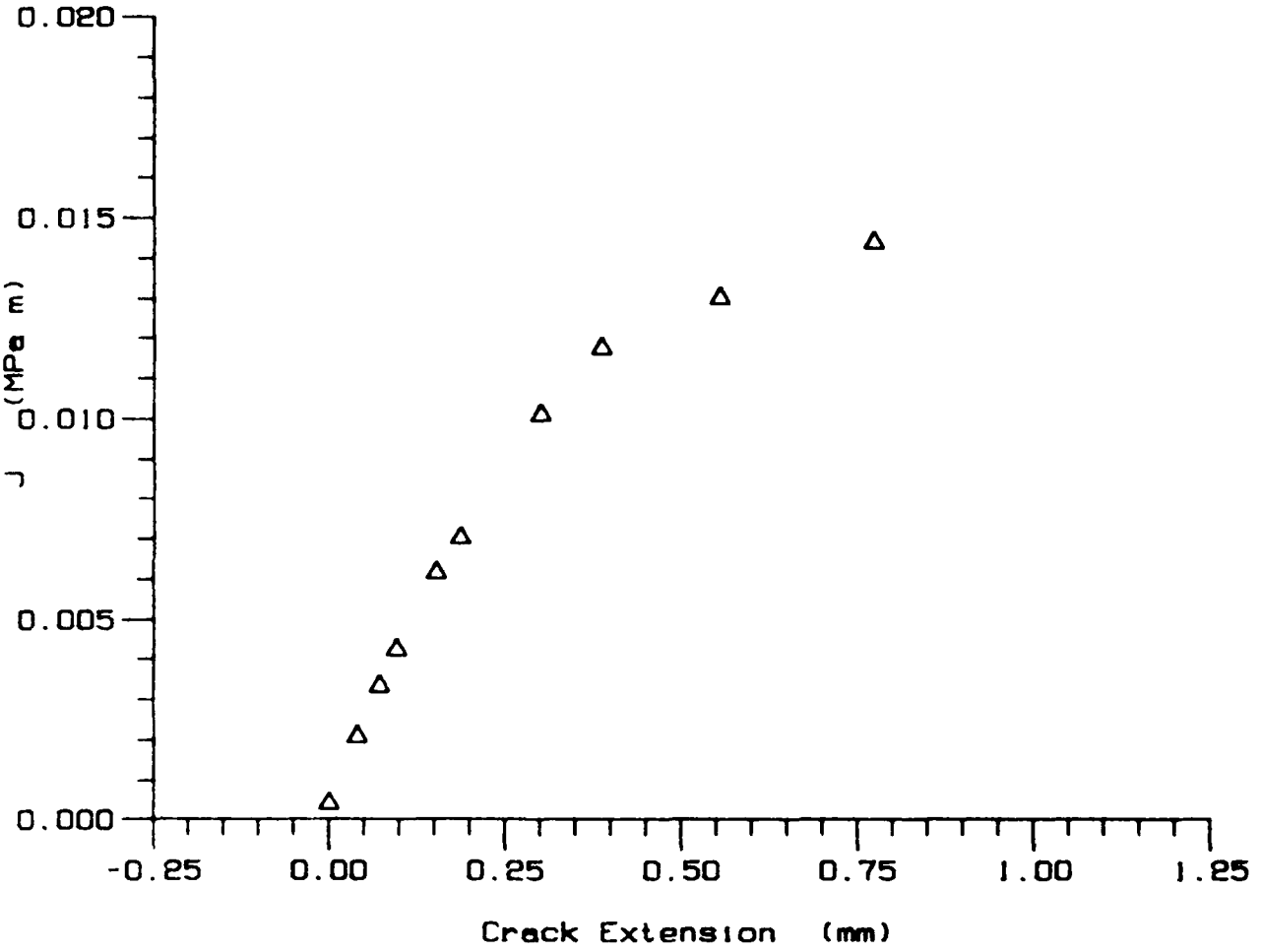

Figure 16 Approximate J Values Versus Crack Extension. 2024-0 Aluminum Fatigue Precracked SEN Specimen. Specimen No. KJC1.

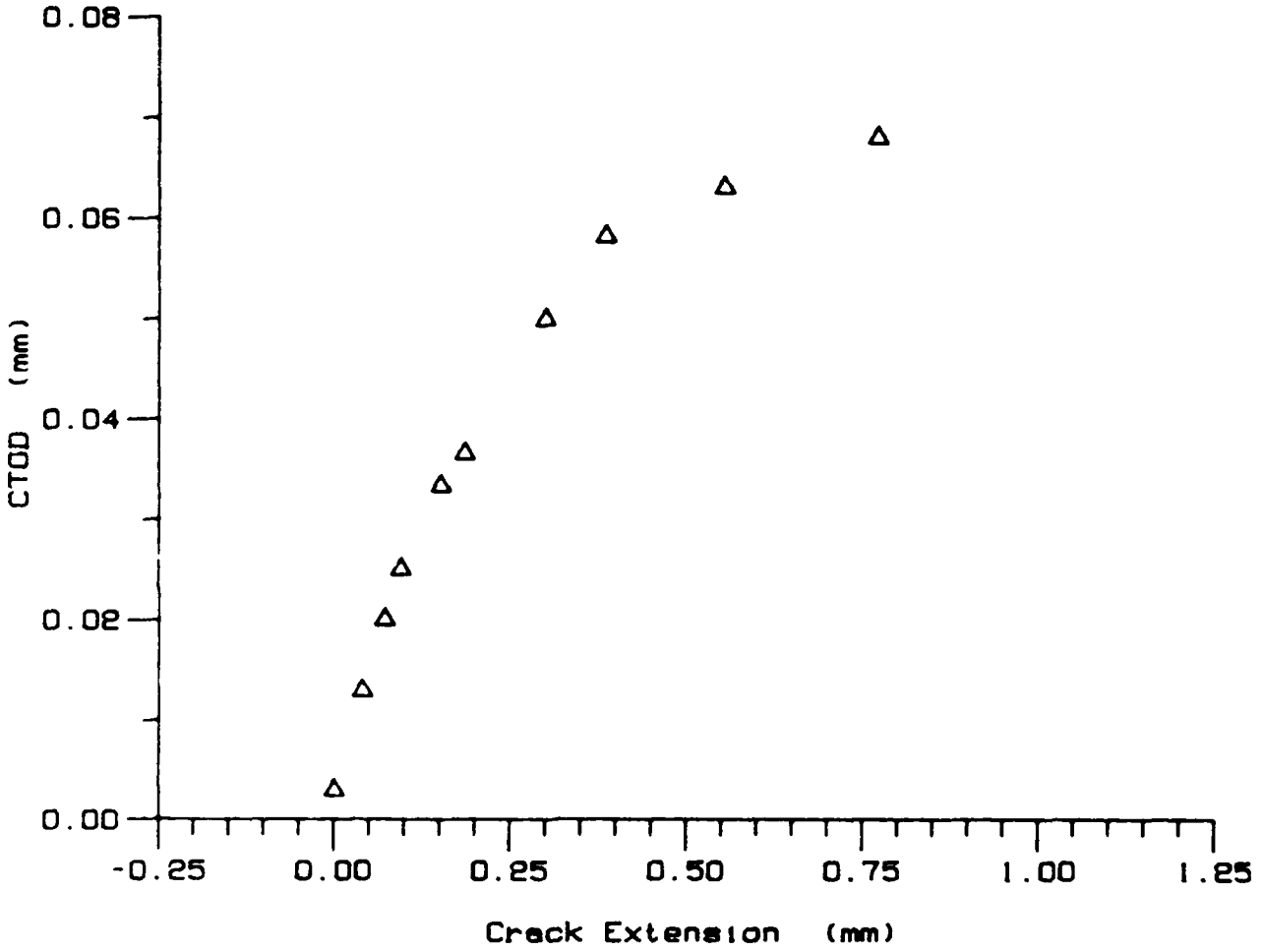

Figure 17 Measured Crack Tip Opening Displacement (CTOD) Values Versus Crack Extension. 2024-0 Aluminum Fatigue Precracked SEN Specimen. Specimen No. KJC1.

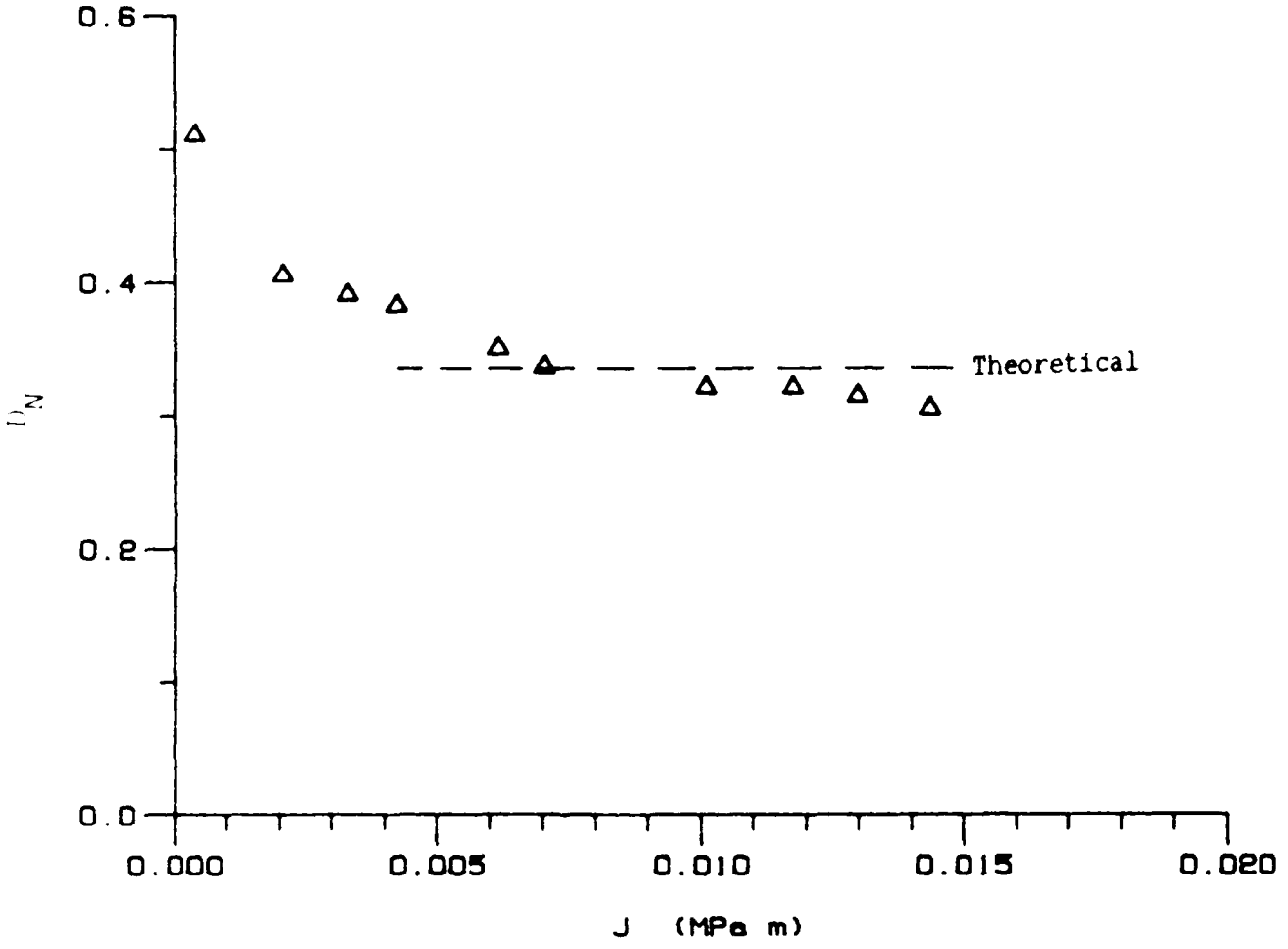

Figure 18 Variation of D_N With Crack Extension. 2024-O Aluminum Fatigue Precracked SEN Specimen; $D_N=\delta_t/(J/\sigma_o)$. Specimen No. KJC1.

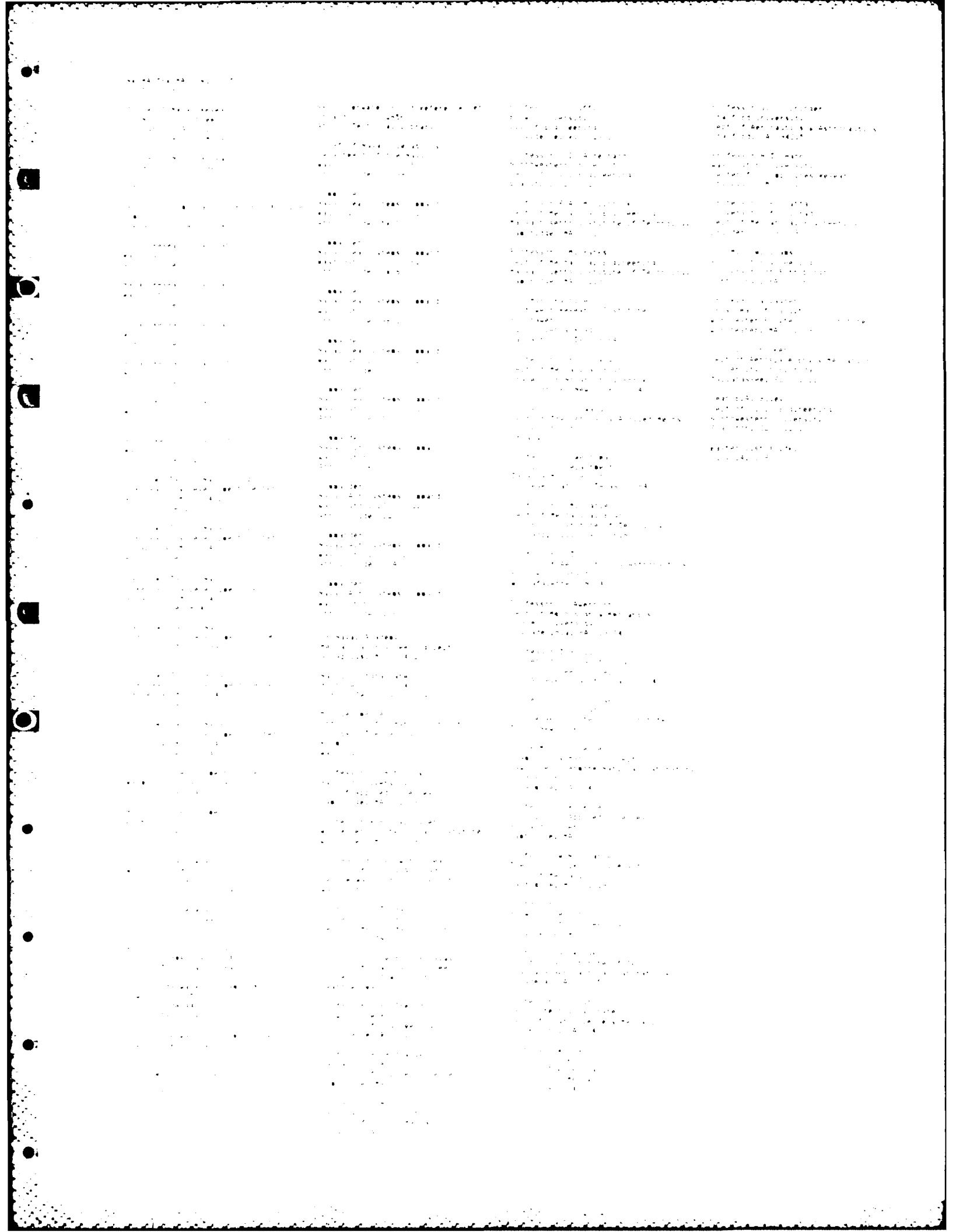

unclassified

SECURITY CLASSIFICATION OF THIS PAGE (When Data Entered)

REPORT DOCUMENTATION PAGE		READ INSTRUCTIONS BEFORE COMPLETING FORM
1. REPORT NUMBER UWA/DME/TR-86/54	2. GOVT ACCESSION NO. AD-A170	3. RECIPIENT'S CATALOG NUMBER
4. TITLE (and Subtitle) Stable Crack Growth in Aluminum Tensile Specimen		5. TYPE OF REPORT & PERIOD COVERED Technical Report
		6. PERFORMING ORG. REPORT NUMBER UWA/DME/TR-86/54
7. AUTHOR(s) B.S.-J. Kang, A.S. Kobayashi, and D. Post		8. CONTRACT OR GRANT NUMBER(s) N00014-85-K-0187
9. PERFORMING ORGANIZATION NAME AND ADDRESS Department of Mechanical Engineering, FU-10 University of Washington Seattle, Washington 98195		10. PROGRAM ELEMENT, PROJECT, TASK AREA & WORK UNIT NUMBERS
11. CONTROLLING OFFICE NAME AND ADDRESS Office of Naval Research Arlington, Virginia 22217		12. REPORT DATE July, 1986 13. NUMBER OF PAGES 38
14. MONITORING AGENCY NAME & ADDRESS(if different from Controlling Office)		15. SECURITY CLASS. (of this report) Unclassifed 15a. DECLASSIFICATION/DOWNGRADING SCHEDULE

16. DISTRIBUTION STATEMENT (of this Report)

unlimited

17. DISTRIBUTION STATEMENT (of the abstract entered in Block 20, if different from Report)

18. SUPPLEMENTARY NOTES

19. KEY WORDS (Continue on reverse side if necessary and identify by block number)

Moire, stable crack growth, J-integral, CTOD, Dugdale strip yield zone

20. ABSTRACT (Continue on reverse side if necessary and identify by block number)

Post's white light moire interferometry was used to obtain sequential records of the transient u_y-displacement fields associated with stable crack growth in 7075-T6 and 2024-0, single end notched (SEN) specimens with fatigued cracks. The u_y-displacement fields were used to evaluate the crack tip opening displacement (CTOD), far and near-field J-integral values, Dugdale strip yield model, William's polynomial function, and the HRR fields.

DD FORM 1473 EDITION OF 1 NOV 65 IS OBSOLETE

S/N 0102-LF-014-6601

SECURITY CLASSIFICATION OF THIS PAGE (When Data Entered)

END

DTIC

8—86